HELSINKI UNIVERSITY OF TECHNOLOGY
Department of Chemical Technology

Mari Aaltonen

THE ELECTROCHEMICAL DISSOLUTION OF ZINC SULPHIDE CONCENTRATES

Thesis for the degree of Master of Science in Technology.

Espoo, 20 February 2002

Supervisor:

Professor Kyösti Kontturi

Instructor:

Pekka Taskinen, PhD.

TEKNILLINEN KORKEAKOULU DIPLOMITYÖN TIIVISTELMÄ
Kemian tekniikan osasto

Tekijä Mari Aaltonen	Päiväys 20.2.2002
	Sivumäärä 70
Työn nimi Sinkkisulfidirikasteiden sähkökemiallinen liukeneminen	
Professuuri Fysikaalinen kemia ja sähkökemia	Koodi Kem-31
Työn valvoja Professori Kyösti Kontturi	
Työn ohjaaja TkT Pekka Taskinen	

Diplomityön kirjallisuusosa käsittelee sinkkisulfidin atmosfääristä, hapettavaa liuotusta ferrisulfaattia sisältävissä rikkihappoliuksissa. Työssä esitellään sinkkisulfidin liuotukseen liittyviä sähkökemiallisia reaktioita sekä yleisesti sulfidimineraalien liuotukseen liittyviä nopeusyhtälöitä ja reaktiomekanismeja. Tässä osassa tutustutaan myös erilaisten muuttujien vaikutukseen liukenemisnopeuteen. Lisäksi esitetään kirjallisuudesta löytyvien sinkkisulfidia koskevien sähkökemiallisten tutkielmien tutkimusmenetelmiä ja tuloksia.

Työn kokeellinen osa sisälsi kuuden tunnin liuotuskokeita jotka suoritettiin hapettomissa, ferrisulfaattia sisältävissä rikkihappoliuksissa. Tutkittavana oli yhtä Outokummun Pyhäsalmen rikastetta, joka oli eritelty neljään kokofraktioon. Tutkimukset suoritettiin 60°C, 70°C, 80° ja 90°C:n lämpötiloissa ja myös sekoitusnopeuden sekä liuenneen sinkin ja raudan konsentraatioden vaikutusta reaktionopeuteen tutkittiin.

Mittautuloksista nähdään, että lämpötilan nosto 60°C:sta 70°C:een nopeuttaa huomattavasti liukenemisreaktiota. Kun lämpötilaa nostetaan edelleen 80°C ja 90°C, näin suurta muutosta ei ole huomattavissa, mikä viitta siihen, että reaktionopeutta rajoittava vaihe vaihtuu. Kuten oli odotettavissa, liukenemisnopeus oli sitä suurempi, mitä pienempi partikkelikoko oli kyseessä. Liuoksen ferrirauta konsentraation nostaminen 33 mM:sta 52 mM:in nosti selvästi myös reaktionopeutta ja konversiota. Kuitenkin konsentraation nostaminen edelleen 75 mM:in sai aikaan vain hienoisen nousun konversiossa. Liuokseen lisätyn liuenneen sinkin (100 g/l) vaikutus lämpötiloissa 70°C, 80°C ja 90°C näkyi 15 % konversion laskuna. Kuudessakymmenessä asteessa konversio yllättäen putosi 67 %. Sekoitusnopeuden muuttamisella 1000 rpm:sta 500 rpm:n ei saatu aikaan huomattavaa muutosta liukenemisnopeudessa. Kaksi nopeusyhtälöä sovitettiin mittausten tuloksiin, ja tulokset viittaavat siihen, että liukenemisen alussa mineraalin pinnalla tapahtuva reaktio määrää liukenemisen nopeuden ja myöhemmissä vaiheissa diffuusio tuotekerroksen läpi on reaktionopeutta rajoittava tekijä.

Liukenemisprosessin samanaikaseen seurantaan ehdotettiin potentiostaattista menetelmää, joka perustuu ferri- ja ferrorautaionien aiheuttaman potentiaalin mittaamiseen. Mittausten aikana mitattiin liuoksen potentiaalia platinaelektrodin ja Ag/AgCl-referenssielektrodin avulla ja konversio ajan funktiona laskettiin näistä tuloksisa. Menetelmän tarkkuuden määrittämiseksi analysoitiin sinkin määrä liuosnäytteissä atomiabsorptiospektrometriaa käyttäen, ja tuloksista laskettuja konversioita verrattiin potentiometrisen määrityksen tuloksiin. Eri menetelmillä lasketut konversiot erosivat toisistaan toistuvasti noin 20 %:lla, mikä saattaa viitata liuoksessa tapahtuvaan toiseen hapetusreaktioon. Elementäärisen rikin hapettuminen sulfaatiksi selittäisi nämä eroavuudet lasketuissa konversioissa. Jatkotutkimuksilla tullaan selvittämään tämän hypoteesin paikkaansapitävyys.

HELSINKI UNIVERSITY OF TECHNOLOGY
Department of Chemical Technology

ABSTRACT OF MASTER'S THESIS

Author
Mari Aaltonen

Date
20.2.2002

Pages
70

Title of thesis
The electrochemical dissolution of zinc sulphide concentrates

Chair
Physical Chemistry and Electrochemistry

Chair Code
Kem-31

Supervisor
Kyösti Kontturi, Professor

Instructor
Pekka Taskinen, PhD

The literature part of this thesis reviewed the theory of atmospheric oxidative dissolution of zinc sulphide concentrates in ferric sulphide media. The electrochemical reactions involved in this dissolution and the rate equations and mechanisms associated with sulphide mineral dissolution in general were presented and the factors affecting the rate of dissolution were discussed. The methods and results of several electrochemical studies on sulphide minerals were summarized.

The experimental part of this work consists of 6 hour dissolution experiments carried out in oxygen-free sulphuric acid solutions containing ferric sulphide. Four size fractions of one Outokumpu Pyhäsalmi concentrate were used and the experiments were conducted at temperatures 60°C, 70°C, 80°C and 90°C. Other variables under study were the rate of stirring and the concentrations of zinc and ferric ions in the solution.

The results of the experiments show, that increasing the temperature from 60°C to 70°C increases the rate of dissolution considerably. Raising the temperature further to 80°C or 90°C had only a slight effect on the rate of dissolution and conversions reached. This would suggest a change in the reaction mechanism. The effect of particle size on the rate of dissolution was not surprising, the rate increased with the decease of particle size. As the iron content in the solution was raised from 33 mM to 52 mM, a significant increase in the conversion was noted, while a further increase to 75 mM had practically no effect. At temperatures 70°C, 80°C and 90°C, the effect of 100 g/l of dissolved zinc in the solution was a 15 % decrease in conversions, at 60°C a decrease of 67 % was unexpectedly seen. No significant change in conversions was reached by decreasing the rate of stirring from 1000 rpm to 500 rpm. Two rate equations were fitted to the experimental data, and the results suggest that the rate of dissolution is first controlled by the reaction taking place at the mineral surface, the diffusion through a product layer becoming the rate-determining step at latter stages of the dissolution.

A potentiometric method for the *in-situ* monitoring of the dissolution process, based on the potential of the ferric/ferrous ion couple, was suggested and tested. During the dissolution experiments, the potential difference between a platinum electrode and a Ag/AgCl reference electrode was measured and conversion of zinc sulphide to dissolved zinc was calculated. To evaluate the accuracy of the potentiometic method, conversions were also calculated from the results of atomic absorption spectroscopy analysis. The parallel analysis show a consistent difference of about 20 % between the conversions indicated by the two methods of analysis. This discrepancy could be explained by the oxidation of elemental sulphur to sulphate, which would affect the ferric/ferrous ion equilibrium in the solution. Further research has to be carried out in order to verify this hypothesis.

Acknowledgements

The work for this thesis was conducted between June 2001 and February 2002 in the Laboratory of Physical chemistry and electrochemistry at the Helsinki University of Technology.

I want to thank Professor Kyösti Kontturi, the supervisor of this thesis, for his ideas, for his input throughout the process and for reminding me every now and then of the beauty of electrochemistry. Similarly I want to thank Pekka Taskinen, PhD., from Outokumpu Research Oy, the instructor of the thesis, for all the knowledge and enthusiasm he brough to this process, as well as for introducing me to the intriguing world of metals. The interest and expertise of Olli Hyvärinen, PhD, (Outokumpu) are also looked upon with gratitude.

I feel privileged to work within such a wonderful work community, and I wish to thank the whole staff of the laboratory of physical chemistry and electrochemistry at HUT for making me always feel at home and amongst friends. Especially I want to express my gratitude to Peter and Roope for always having time to help me out, whether by proof reading this thesis or by acting as an arbitrator between me and my computer (or anyone else's for that matter).

Most of all I want to thank my parents, my sister and my tiny brother for helping me through the tough times with their infinite encouragement, humour and love. A big thank you goes also to my friends for always being there for me. This thesis would never have seen daylight without your help.

20th Fabruary, 2002

Mari Aaltonen

TABLE OF CONTENTS

LIST OF SYMBOLS

A	the pre-exponential factor (equation 6)	
A_0	the total initial area available for reaction (equation 7)	[m^2]
b	the stoichiometric coefficient (equations 2 and 4)	
c_{fs}	the concentration of Fe^{3+} in the sulphur layer (equations 2 and 4)	[mol/l]
D_e	the effective diffusion coefficient of ions in porous medium (equation 4)	[cm^2/min]
E^0	the standard electrode potential of the reaction	[V]
E_a	the activation energy	[kJ/mol]
E_{ac}	the ionisation energy of the acceptor	[kJ/mol]
E_d	the ionisation energy of the donor	[kJ/mol]
E_f	the Fermi level energy of the semiconductor	[kJ/mol]
E_h	the redox potential of the solution vs. Ag/AgCl (equation 7)	[V]
F	the Faraday constant	[C/mol]
j	the current density (equation 13)	[mA/cm^2]
j_0	the exchange current density (equation 13)	[mA/cm^2]
k_B	the Bolzmann constant	[J/K]
k_c	rate constant of the reaction (equation 6)	
K_c	the rate constant for the surface reaction (equations 1 and 2)	[min^{-1}]
K_{cc}	the chemical rate constant (equation 2)	[cm/min]
K_d	the rate constant for diffusion	[min^{-1}]
M	the amount of leachable material remaining in particle cores (equation 7)	[mol]
M	the molecular weight of sulphide mineral (equations 2 and 4)	[g/mol]
M_0	the initial value of M (equation 7)	[mol]

n	the number of electrons in a unit reaction (equations 9-12)	
N_a	the amount of acceptor atoms (equation 14)	
N_{a-}	the amount of ionised acceptor atoms (equation 14)	
r_0	the radius of the unreacted particle (equations 2 and 4)	[cm]
R	the conversion (equations 1 and 3)	
R	molar gas constant	[J/(mol K)]
t	the reaction time	[min]
T	the absolute temperature	[K]
z	the charge number (equation 13)	
a_{ox}	the product of the activities of the products (equation 12)	
a_{red}	the product of the activities of the reactants (equation 12)	
α	the transfer coefficient (equation 13)	
η_a	the activation overpotential (equation 13)	[V]
ΔG^0	the standard Gibbs free energy of reaction	[kJ/mol]
ρ_z	the density of sulphide mineral (equations 2 and 4)	[g/cm^3]
[*Fe(II)*]	the concentration of Fe^{2+}	[mol/l]
[*Fe(III)*]	the concentration of Fe^{3+}	[mol/l]
[H^+]	the concentration of H^+	[mol/l]
[O_2]	the concentration of O_2	[mol/l]

Abbreviations

AAS	atomic absorbance spectroscopy

1. INTRODUCTION

Zinc is the fourth most used metal in the world today, with a production of 7.5 million tonnes per year. It is mainly used for the galvanisation of metal and in alloys such as brass. Outokumpu Oy produces high purity zinc in Kokkola, Finland, with an annual production 225 000 tonnes and in Outokumpu Norzink in Odda, Norway with a production of 150 000 tonnes per year [1]. The Kokkola plant uses the traditional roasting process alongside with a more modern method of direct atmospheric oxidative leaching [2].

Zinc is mostly mined as sphalerite, a zinc sulphide ore with iron as the main impurity. The traditional zinc refining technique is to burn the ore with air in a fluidised bed reactor at 950°C to form ZnO, which readily dissolves in sulphuric acid. The dissolved zinc is then electrolytically refined. In addition to the common problems of high temperature processes, such as high material costs, the sulphur in the ore causes a problem in the roasting process. The sulphur burns to sulphur dioxide, which has to be used up in another process, as it is not permitted in emission gases and it cannot economically be transported elsewhere. The sulphur dioxide is mostly made into sulphuric acid, the manufacture of which is not profitable in many cases due to overproduction. The advantage of oxidative leaching is that it produces solid elemental sulphur, which is easily stored, instead of gaseous SO_2. The use of both processes together also allows for the best method to be chosen for each kind of concentrate. For example, finely ground concentrates and concentrates containing high concentrations of lead or copper are best processed through direct leaching, while roasting is more suitable for concentrates containing traces of mercury or high concentrations of chloride. [3]

2. CHEMICAL REACTIONS IN ZINC SULPHIDE LEACHING

2.1 Atmospheric ferric sulphate leaching

The dissolution of ZnS in aqueous solutions is an electrochemical process, taking place through the coupled reactions of reduction and oxidation. In the Kokkola atmospheric dissolution process, aqueous sulphuric acid is used as the solvent and ferric ions as the oxidising agent at temperatures close to 100°C. The first redox reaction in ferric sulphate dissolution of ZnS is [4]:

$$ZnS\,(s) + 2\,Fe^{3+}\,(aq) \rightarrow Zn^{2+}\,(aq) + 2\,Fe^{2+}\,(aq) + S\,(s) \qquad (R1)$$

The dissolved Zn^{2+} ions are reduced to pure zinc in an electrolytic process. The Fe^{2+} ions are oxidised back to the reactive Fe^{3+} by oxygen in the second redox reaction:

$$2\,Fe^{2+}\,(aq) + H_2SO_4\,(aq) + ½\,O_2\,(g) \rightarrow 2\,Fe^{3+}\,(aq) + SO_4^{2-}\,(aq) + H_2O \qquad (R2)$$

Combining these two reactions gives the total reaction for the dissolution:

$$ZnS\,(aq) + H_2SO_4\,(aq) + ½\,O_2\,(g) \rightarrow ZnSO_4\,(aq) + S\,(s) + H_2O \qquad (R3)$$

At high potentials, $E^0 = 0.12$ V for sphalerite compact in 0.5 mol/l sulphuric acid according to Srinivasan et al.[5], elemental sulphur can oxidise further to sulphate ions:

$$S\,(s) + 6\,Fe^{3+}\,(aq) + 4\,H_2O \rightarrow 8\,H^{+}\,(aq) + SO_4^{2-}\,(aq) + 6\,Fe^{2+}\,(aq) \qquad (R4)$$

Small amounts of lead are present in many sphalerite ores. During dissolution, the lead has been shown to stay in the deposit as PbS or $PbSO_4$, since analysis of the solvent in dissolution studies show only minimal amounts of dissolved lead. [6]

The conversion slurry fed to the oxidative leaching process contains iron in the form of jarosite. In the beginning of oxidative dissolution the acid level is higher than at the previous unit process, and some of the jarosite dissolves. In the end of the dissolution process, the concentration of sulphuric acid decreases and iron is precipitated again as jarosite:

$$1½\ Fe_2(SO_4)_3 + ½\ (NH_4)_2SO_4 + 6\ H_2O \rightarrow NH_4Fe_3(SO_4)_2(OH)_6 + 3\ H_2SO_4 \quad (R5)$$

The cation in jarosite is not necessarily NH_4^+, it can also be some other cation from the solution, for example K^+, Na^+, Pb^{2+} or H_3O^+.[2]

2.2 Pressure leaching

Before atmospheric leaching was implemented, pressure leaching was an alternative to the roasting-leaching process. The advantages and methods of direct pressure leaching of ZnS were reviewed by Veltman *et al.* [7]. Results of studies conducted under pressure leaching conditions are referred to and built upon throughout articles concerning atmospheric leaching, although these studies utilised both higher pressure and temperature.

In 1976 Jan *et al.* [8] concluded from their kinetic study of ZnS oxidative pressure leaching that the dissolution of sphalerite did not take place through direct oxidation by molecular oxygen, but by a reaction with ferric ions in the solution. They also found the rate-limiting step to be the oxidation of hydrogen sulphide to elemental sulphur. This was later supported by other researchers such as Courriou *et al.* [9] who conducted a vast study of the thermodynamics and kinetics of ZnS dissolution in sulphur acid under pressure leaching conditions. The study included two empirical kinetic models of the dissolution phenomenon and calculations of activation energies, activity coefficients and reaction enthalpies. An equation describing the oxidation of ferrous sulphate by oxygen in pressure leach conditions was presented by Dresinger *et al.* [10]. Equations derived from the results of pressure leaching studies cannot directly be applied to atmospheric leaching conditions, but do give a basis for understanding the phenomena.

2.3 Ferric chloride leaching

Many studies of atmospheric sphalerite leaching have been conducted in ferric chloride solutions. Dutrizac *et al*. [11] as well as Zuo-Mei Jin *et al*. [12] concluded that the dissolution reaction in ferric chloride media is kinetically controlled. Bobek *et al.* [13] proposed that during the initial stages of leaching, the reaction is chemically controlled, while at a latter stage diffusion through a sulphur product layer becomes the rate-determining step. Suni *et al*. [14] derived a model for the batch-leaching behaviour of multisize sphalerite concentrates in ferric chloride solutions, based on the surface limiting expression for mineral dissolution further discussed in section 3.1.

2.4 Electrobioleaching

The electrobioleaching of ZnS and other sulphide minerals has been the subject of several recent studies [15], [16]. The effect of the most studied bacteria *thiobacillus ferroxidans* can be through direct dissolution of the sulphide or by regeneration of the ferric ion to the oxidising ferrous ion. Fowler *at al.* [17] found that *thiobacillus ferroxidans* oxidises the elemental sulphur layer and thus enables the diffusion of ferric ions to the reactive mineral surface.

3. THE RATE AND MECHANISMS OF DISSOLUTION

3.1 The shrinking core model

ZnS dissolution follows the shrinking core model, in which dissolution products form on the surface of the mineral and the dissolution continues by diffusion through this layer. The diameter of the particle remains constant, but the area of the surface where the reaction can take place decreases with time. [18], [19], [20] The shrinking core model is depicted in figure 1:

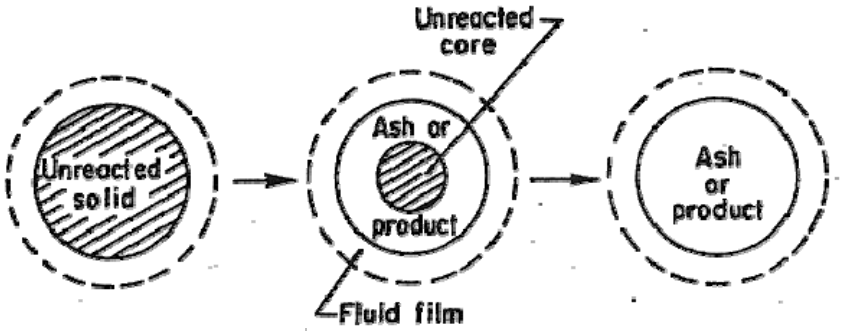

Figure 1. The shrinking core model. [3]

The kinetic steps involved in shrinking core dissolution are:

1. The mass transfer of reagents and products through the solution, between the particle surface and the bulk solution
2. The diffusion of reagents and products through the product layer in the particle, between the surfaces of the particle and the reacting core
3. A chemical reaction
4. A charge transfer reaction.

Theoretically any of these steps can be rate limiting, determining the overall rate of dissolution. However, depending on the process variables, some of these factors can be inconsequential. For example, in some studies of zinc dissolution, no rate determining chemical reactions have been considered, due to the

electrochemical nature of the dissolution process. In some cases, the effects of mass transfer in the solution can be discarded while applying adequate mixing, although particle size and shape also have to be taken into account.

3.1.1 Surface reaction control

In the beginning of dissolution, the reacting surface of the mineral is free from product layers, and the rate-limiting step is the charge transfer reaction. For the case of total surface reaction control, the rate of reaction is expressed by equation (1) [13], [20], [21], [22]:

$$K_c t = 1 - (1 - R)^{1/3} \tag{1}$$

where t is the reaction time, R is the conversion, given by $1 - (r/r_0)^3$ and K_c is the rate constant for the reaction, given by (2) [13]:

$$K_c = \frac{MbK_{cc}c_{fs}}{r_0 \rho_z} \tag{2}$$

where M is the molecular weight of the sulphide mineral, b is the stoichiometric coefficient, K_{cc} is the chemical rate constant, c_{fs} is the concentration of Fe^{3+} in the sulphur layer on the mineral surface, r_0 is the radius of the unreacted particle and ρ_z is the density of sulphide mineral. [13]

Crundwell [18] suggested that sphalerite dissolution in sulphuric acid with ferric sulphate obeys the reaction controlled shrinking core mechanism. The results of dissolution experiments of sphalerite in ferric sulphide and ferric chloride media by Palencia Perez *et al.* [23] support this theory. Lapidus *et al*. [24] proposed an extension to the shrinking core model, which could take into consideration mass transfer of the dissolution products through the liquid film, as well as, the effect of metal solubility on the rate of dissolution, resulting in a more complex kinetic equation. Their experiments of ammoniacal leaching of zinc with cupric chloride support the theory of product diffusion control.

3.1.2 Diffusion control

As dissolution advances, a layer of products is formed on top of the reacting core and the rate of dissolution is limited by diffusion through this layer. For this case the Crank-Ginstling and Brounstein model for diffusion through a non-porous product layer [13], [20], [22] can be used to determine the reaction rate:

$$K_d t = 1 - \frac{2}{3} R - (1 - R)^{2/3} \tag{3}$$

where K_d is the rate constant for diffusion, given by (4) [13]:

$$K_d = \frac{2MbD_e c_{fs}}{r_0^2 \rho_z} \tag{4}$$

where D_e is the effective diffusion coefficient of ions in porous medium.

Munoz *et al.* [25] found that chalcopyrite reacts similarly to sphalerite under acidic ferric sulphate dissolution conditions, and a layer of elemental sulphur is formed on the reaction surface. They defined the rate determining steps to be the diffusion of electrons and dissolved ions through this layer. Choi and Torma [26] investigated the electrochemical reactions involved in oxidative leaching of ZnS in sulphuric acid, with and without bacteria, or in hydrochloric acid with ferric chloride. Their cyclic voltammetry measurements show a multi-reaction mechanism and in their chronoamperometric and chronopotentiometric studies they show the leaching process to be controlled by solid-state diffusion.

3.1.3 Joint control

In the beginning of dissolution the rate of reaction is mainly governed by the electrochemical surface reaction, but as the sulphur layer grows thicker, the effect of diffusion through the product layer becomes more pronounced. In effect, these

limitations should be considered together, resulting in the rate equation (5) [13], [24]:

$$\frac{MbK_{cc}D_e c_{fs}}{r_0^2 \rho_z} t = \frac{D_e}{r_0}\left[1-(1-R)^{1/3}\right] + \frac{K_{cc}}{2}\left[1-\frac{2}{3}R-(1-R)^{2/3}\right] \quad (5)$$

It has been estimated that in ZnS dissolution, the charge transfer reaction determines the rate of reaction until 50-70% conversion is reached, after which both charge transfer and diffusion through a product layer have to be taken into account. [3]

3.2 Activation energies and the effect of temperature

E_a , the activation energy of a reaction, represents the effect of temperature on the rate of reaction. This relation between temperature and the rate of reaction is given by the Arrhenius equation [27]:

$$k_c = Ae^{(-Ea/RT)} \quad (6)$$

where k_c is the rate constant of the reaction, A is the pre-exponential factor, E_a is the activation energy, R is the molar gas constant and T is the absolute temperature.

The higher the activation energy, the more effect temperature has on the rate of reaction. Diffusion is moderately dependent on temperature, and the activation energies for diffusion through a liquid film are 4.2-12.6 kJ/mol [3]. Chemical reactions usually have activation energies greater than 40 kJ/mol [3], and are highly dependent on the temperature. When the rate-limiting step is diffusion through a porous layer, the apparent activation energy lies between these the two ranges of values.

A variety of different activation energy values have been reported for sulphide dissolution reactions. In oxidative ZnS dissolution experiments, Halavaara [28] found that as temperature was raised from 60°C to 90°C the rate of dissolution

grew tenfold. From the initial rates of reaction activation energies were calculated to be 30 kJ/mol at temperatures 50°C - 80°C and 74 kJ/mol at 80°C - 100°C. Bobek *et al.* [13] calculated an overall activation energy of 46.9 kJ/mol for sphalerite dissolution reaction, with an A_e of 50 kJ/mol in the initial stages of dissolution, consistent with a kinetically controlled reaction.

Munoz *et al*. [25] studied the acid ferric sulphide dissolution of chalcopyrite, which has a similar shrinking core mechanism, with an elemental sulphur layer, as sphalerite. The activation energy for the dissolution was measured as 83.7 kJ/mol, which corresponds reasonably with the activation energy for electron conductivity in elemental sulphur, 96.3 kJ/mol. This would suggest the electron conductivity of the product sulphur layer to be the rate-limiting step.

3.3 The effect of iron on the rate of dissolution

The amount of iron in the sphalerite ore has been shown to have a strong effect on the rate of dissolution. Bobek *et al.* [13] report that the presence of iron in sphalerite mineral increases the rate of the dissolution reaction. Also experiments by Halavaara [28] suggest the rate of reaction to increase as a function of iron content of the zinc concentrate. In the latter study the rate enhancing effect of iron was found to cease as diffusion through the product layer became the rate-determining step.

Pelencia Perez *et al*. [23] studied the effect of iron content of sphalerite on the dissolution rate and found the relation to be linear. They summarised the results of four other studies which, combined with their own, show that in ferric sulphate-sulphuric acid media the rate of reaction increases by 25 %-135 % as the iron content is increased by 1 %. Kemmel *et al.* [29] found the equilibrium potential of sphalerite to be greatly decreased with increasing iron content of the mineral. They also show that the catalytic effect of Cu^{2+} in ZnS leaching is dependent on the iron content of the lattice: for minerals with iron contents under 1%, the addition of Cu^{2+} increases Zn extraction, while the extraction rate of minerals with a higher iron content is reduced. It was suggested, that on the surfaces of a low

iron-content mineral CuS be formed, while Cu_2S is formed on minerals with a high content of iron.

Crundwell [18] found that the addition of Fe^{2+} ions into solution decreased the rate of sphalerite dissolution. The rate decreasing effect was explained by an indirect mechanism, in which the Fe^{2+} ions affect the concentrations of the oxidative species, Fe^{3+} and $FeHSO_4^{2+}$, in the solution. Crundwell [19] also studied the uncommonly low conversion rates of two sphalerite minerals of high lead content. He proposed the formation of a dissolution limiting layer of $PbSO_4$ or lead jarosite, which both are insoluble in sulphate solutions. This theory was supported by results, which show no passivation of the sphalerite surfaces in chloride solutions, in which basic lead sulphates are soluble.

Verbaan and Crundwell [30] derived an electrochemical kinetic model for the leaching of sphalerite in acidic ferric sulphate solution. For the particular sphalerite concentrate studied, the dissolution rate was expressed by (7):

$$-\frac{dM}{dt} = 6.505\frac{mol}{l \cdot s}\exp\left(\frac{-79.4J/mol}{RT}\right)\frac{A_0}{m^2}(M/M_0)^{2/3}\exp\left(\frac{17.3}{V}E_h\right) \qquad (7)$$

where M is the amount of leachable material remaining in particle cores, M_0 is the initial value of M, A_0 is the total initial area available for reaction and E_h is the redox potential of the solution vs. Ag/AgCl.

The rate of ferrous-ion oxidation was expressed by (8):

$$\frac{d[Fe(III)]}{dt} = 2.08 \cdot 10^9 \frac{l^{1.65}}{mol^{1.65} \cdot s}\frac{[Fe(II)]^2[O_2]}{[H^+]^{0.35}}\exp\left(\frac{-68.6J/mol}{RT}\right) \qquad (8)$$

where $[Fe(III)]$ is the concentration of Fe^{3+}, $[Fe(II)]$ is the concentration of Fe^{2+}, $[O_2]$ is the concentration of O_2 and $[H^+]$ is the concentration of H^+.

As shown in figure 2, experimental results were explained well by an expression for the combined leaching process, derived by the simultaneous integration of these equations.

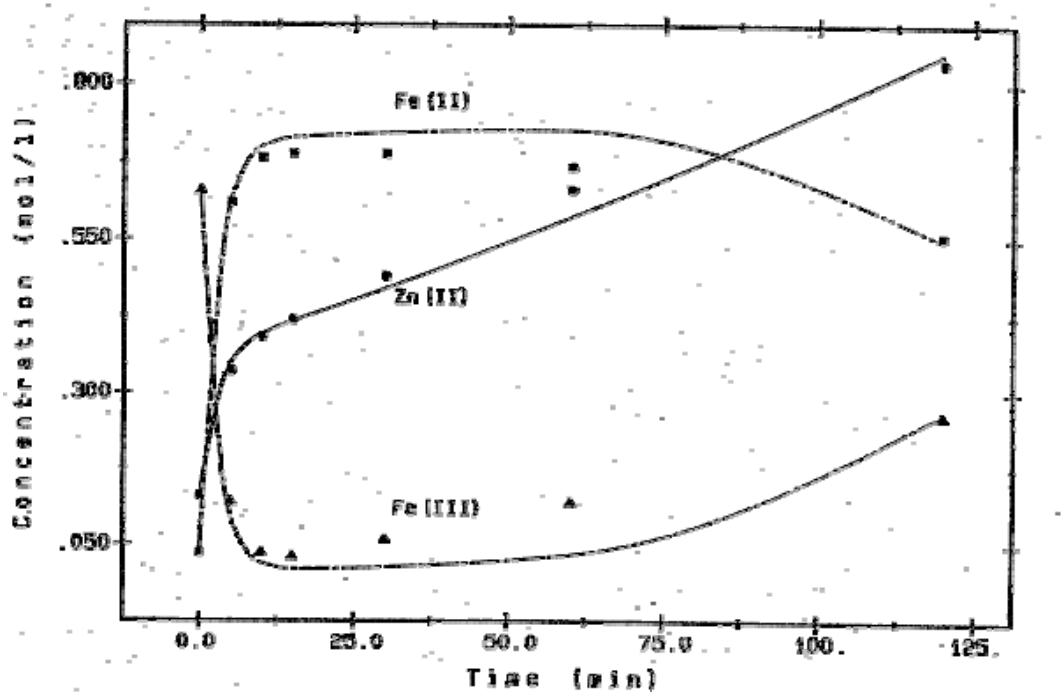

Figure 2. Prediction of the leaching of sphalerite for Zn(II), Fe(II) and Fe(III) in the presence of oxygen, at 90℃. The points are measured, lines calculated from equations (7) and (8). [30]

3.4 Effects of ore composition, particle size, stirring and mechanical activation on the rate of dissolution

Kantanen [6] studied how the composition of a zinc concentrate affected the rate of dissolution in sulphuric acid. Dissolution experiments were carried out with 22 different ore samples. Under study were the rates of dissolution, the amount of zinc dissolved and the effects of different variables on the reaction rates. Analyses were made of the Zn, Fe, Fe^{2+}, Fe^{3+} and H_2SO_4 concentrations in the solution and the Zn, Pb and Fe concentrations in the deposit. Results from the 5 h and 24 h dissolution tests show that the conversions of the different ores differ considerably

at 5 hours but are much more alike after 24 hours. The ore composition was shown to greatly affect the rate of dissolution only in the beginning of dissolution.

Rytioja [3] also performed dissolution tests in ferric sulphate/sulphuric acid solutions on various ZnS concentrates. The rate of dissolution was found to be faster at the beginning of the experiment for the ores with higher final yields, compared to ores of smaller final yields. No clear correlation was found between chemical composition of the concentrate and the final yield of Zn. However, small particle size was found to correlate with better yield compared to samples of large particle size.

In measurements made by Halavaara [28], the initial rate of ZnS dissolution in sulphuric acid was found to be inversely proportional to the radius of the particle, and the rate of reaction was shown to increase as a function of surface area. It was also stated, that the rate of stirring did not noticeably affect the rate of the ZnS dissolution reaction. This result is in contrast with the results of Palencia et al. [31] and Haung et al. [4], who found the dissolution rate to increase with more efficient stirring. However, this difference could be explained by a difference in particle sizes. As the size of a particle decreases, diffusion to the particle surface becomes more spherical and the effect of stirring becomes less pronounced.

Takala [2], [21] reported ZnS dissolution rate in sulphuric acid to be effected by the particle size distribution, and the growth of Zn concentration in concentrate to decrease zinc conversion. The effects of zinc concentration, oxygen pressure, temperature and sulphuric acid concentration on the kinetics of zinc sulphide non-oxidative dissolution in sulphuric acid were studied by Gely *et al*. [32]. They found that when no oxidation agent was present, the formation of H_2S inhibited the dissolution reaction and activated carbon could be used to accelerate the reaction by absorbing H_2S. When oxygen was present, it oxidised the H_2S to water and elemental sulphur.

Balaz *et al*. [33] found mechanical activation by grinding to increase the rate of sphalerite dissolution in hydrogen peroxide. Kammel *et al*. [29] reported an increase in zinc extraction from 68% to above 95% by grinding sphalerite to

smaller particle size before leaching with sulphuric acid. Grinding increases not only the surface area, but also the amount of lattice defects in the mineral, which can affect both the conductivity and stability of the crystals. Electrical conductivity is an essential factor in determining the rate of sulphide dissolution, as is the diffusion coefficient of the metal ion in the sulphide lattice [34]. The theory and the effects of conductivity and lattice defects are further discussed in section 5.

4. THERMODYNAMICS OF DISSOLUTION

4.1 Thermodynamic stability

The thermodynamic stability of a material can be demonstrated with a Pourbaix-diagram, as a function of pH and potential. The diagrams show under which conditions a reaction can take place, but give no information on the rate of reaction. Figure 3 is a Pourbaix-diagram for the system Zn-S-Fe-H_2O at 100°C, drawn with Outokumpu Oy's HSC Chemistry software:

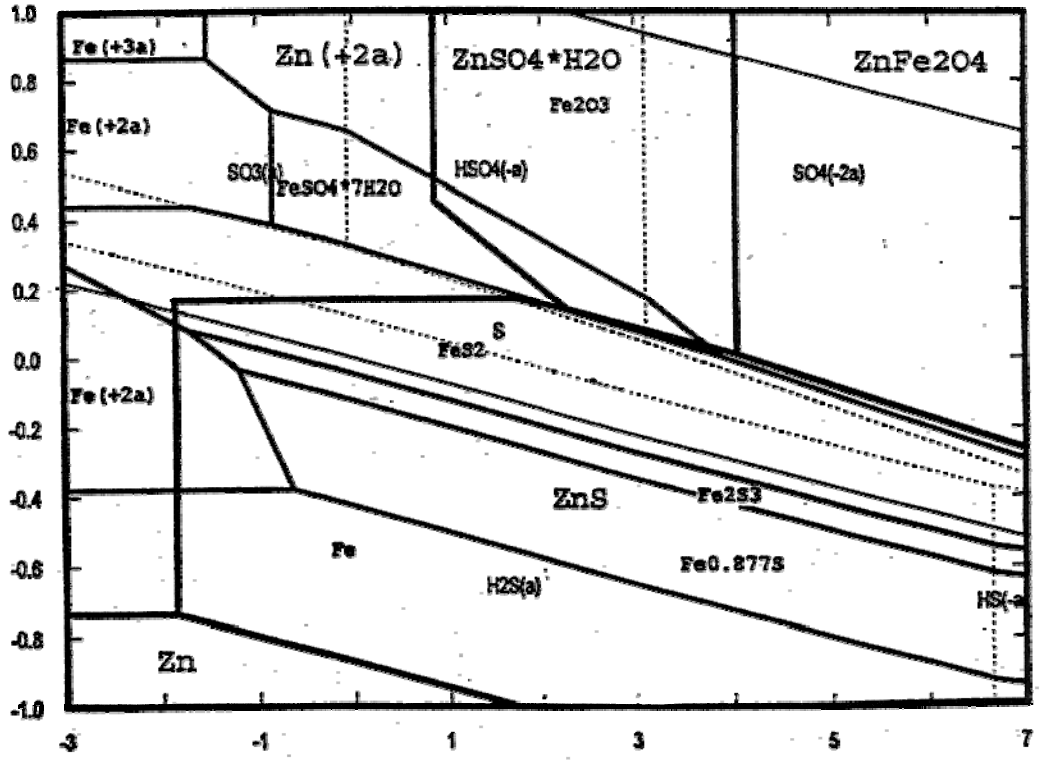

Figure 3. A potential (V) versus pH diagram for the system Zn-S-Fe-H_2O at 100℃, with molalities 1.55 mol Zn / kg , 3.1 mol S / kg and 0.25 mol Fe / kg. [3]

Metastable, operational, equilibrium diagrams are also used. The thermodynamic driving force of a dissolution reaction is the potential difference between the anodic and cathodic reactions, for example the difference between the equilibrium potential of a sulphide and the redox-potential of the solution. [35]

4.2 Electrochemical potentials

Every electrochemical reaction has a given equilibrium potential. Anodic reactions can only take place at potentials above the equilibrium potential and cathodic reactions at potentials below it. The standard electrode potential is related to the reaction's standard Gibb's free energy of reaction according to equation (9):

$$\Delta G^0 = -nFE^0 \tag{9}$$

where ΔG^0 is the standard Gibbs free energy of reaction, n is the number of electrons in a unit reaction, F is the Faraday constant and E^0 is the standard electrode potential of the reaction. [36]

Anodic reactions release electrons, which are needed for a cathodic reaction to occur. The Gibbs energies for associated anodic oxidisation and cathodic reduction are equal and opposite in sign, the standard electrode potential is equal in both cases:

Cathodic reaction: $\Delta G = -nFE$ (10)

Anodic reaction: $\Delta G = nFE$. (11)

The standard potential of a reaction at an electrode/electrolyte interface in real solutions, where activities are not equal to unity and/or temperature differs from the standard 25°C, is given by the Nernst equation (12):

$$E = E^0 + \frac{RT}{nF} \cdot \ln \frac{a_{ox}}{a_{red}} \tag{12}$$

where a_{ox} is the product of the activities of the products and a_{red} is the product of the activities of the reactants. [36]

Many metal sulphides can be made into electrodes, which enables the study of their properties by electrochemical methods. Many factors affect the electrode potentials of metal sulphides, such as the concentration of dissolved metal ions in the electrolyte, the instant dissolution of some ions when immersed in the solvent and the nonstoichiometry of binary sulphides. In kinetic studies it has to be taken into consideration that when the redox reactions are slow, and form metastable intermediates and the potential will affect the reaction kinetics. [37]

During oxidative dissolution of sulphide minerals, the various oxidation steps occurring determine the electrode potentials. As electrons move from the sulphide lattice, chemical bonds are broken and the electron configurations of the lattice atoms are changed, forming layers of varying stoichiometry as depicted in Figure 4:

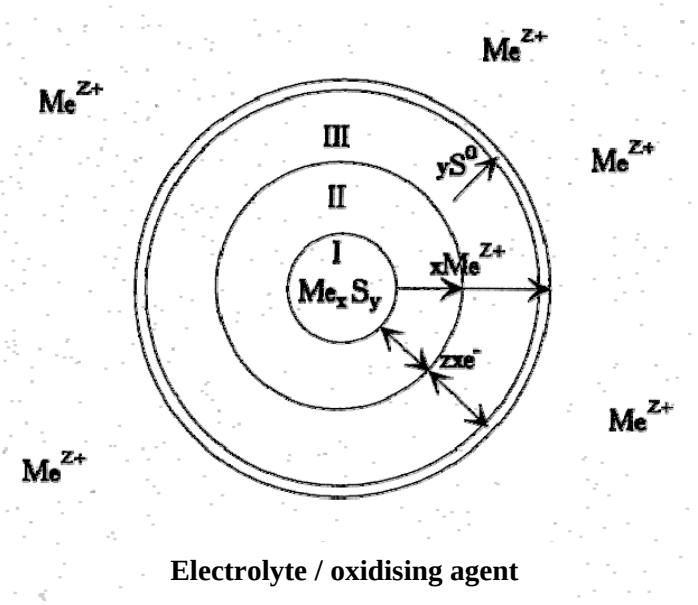

Figure 4. A simplified model of the oxidative dissolution of a binary metal sulphide. [35]

The core, phase I, consists of the original binary mineral sulphide. As the dissolution begins, metal ions from phase I move to the solution and phase II, a metal deficient sulphide is formed. A higher potential is needed for the dissolution of phase II than of phase I. As dissolution continues, a layer of metal deficient sulphide with elemental sulphur, phase III, is formed and this layer has a yet

higher dissolution potential. The outermost layer is of pure elemental sulphur formed as all metal ions have moved to the solution. For dissolution to continue after each step, an increasing potential is required and the layers formed have to enable mass and charge transfer through them. As the sulphur layer grows, it becomes more impenetrable and eventually the dissolution ceases. [35]

In study by Buckley *et al.*[38], it was proposed that in the first stages of sphalerite dissolution in acid, copper ions are transported from the bulk of the mineral to the metal-deficient sulphide layer at the surface. They suggested that the copper sulphide layer, instead of an elemental sulphur layer, causes the decrease in the rate of dissolution. The copper could be removed from this layer by addition of ferric ions in the solution, which is consistent with the known catalytic effect of the Fe^{3+} species. Also lead was found to form passivating layers on a sphalerite surface in sulphate media. The layers were identified as lead sulphate and lead jarosite and were not present in chloride media.

4.3 Mixed potentials

When the anodic and cathodic reactions are in equilibrium the state of the system is described by mixed potential. [39] The anodic and cathodic reactions taking place during oxidative metal sulphide dissolution by ferric-ion are:

Anode: $S^{2-} \rightarrow S^0 + 2\ e^-$ (R6)

Cathode: $2\ Fe^{3+} + 2\ e^- \rightarrow 2\ Fe^{2+}$ (R7)

The separate equilibrium potentials for the half-cell reactions are independent of the electrode surface properties, but these properties affect the shape of the current-potential curve, thus making the mixed potential dependent on them [37]. The anodic overpotential is the difference between the mixed potential and the potential of the anode and is always positive, and similarly the cathodic over potential is the difference between the mixed potential and the potential of the cathode and is always negative. The Butler-Volmer equation (13) can be used to

describe simple charge transfer processes and to link together measured currents and overpotentials. [27]

$$j = j_0\left[\exp(\frac{\alpha zF}{RT}\eta_a) - \exp(\frac{-(1-\alpha)zF}{RT}\eta_a)\right] \quad (13)$$

where j is the current density, j_0 is the exchange current density, α is the transfer coefficient and η_a is the activation overpotential.

In the case of a dissolution reaction, two different mixed potentials can be formed: one from a corrosion reaction and one from a galvanic pair. In a corrosion reaction, the anode and the cathode are parts of the same conductive surface. When two or more phases are in electronic contact with each other a galvanic pair is formed, each phase forming an anode or a cathode. When two different minerals form a galvanic pair, the one with the lower equilibrium potential becomes the anode and dissolves, the other being cathodically protected, supporting only the reduction of the oxidising agent [31].

Zinc sulphide minerals mixed with graphite form a galvanic pair in which the zinc is dissolved. The graphite increases conductivity in the mixture and is favourable to the formation of sulphur crystals [37]. The addition of copper to ZnS forms a galvanic pair ZnS-CuS on the mineral surface, which has been shown to accelerate the anodic dissolution of ZnS [3]. Sphalerite in galvanic interaction with manganese dioxide (pyrolusite) becomes the anode with pyrolusite as the cathode. In a study by Madhuchhanda *et al.* [40], the dissolution of both components was found to increase due to the potential difference. Minerals form the cathode when coupled to metal alloys and enhance the corrosion of the metal [41]. While corrosion reactions and galvanic pairs involving sulphide minerals can be described by mixed potentials, dissolution kinetics of many of these minerals are better described by the semiconductor model discussed in section 5.1.3 [42].

4.4 Electrochemical studies of metal sulphide dissolution

Zhang *et al.* [43] used cyclic voltammetry to study the electrochemistry of the dissolution process of carbon paste-ZnS electrodes in $HCl/FeCl_3$ solutions. The different stages of reduction and oxidation could clearly be seen as separate peaks in the voltammogram, pictured in figure 5, supporting the assumption of an electrochemical process. Peak P_1 represents oxidation of the sulphide to elemental sulphur, P_2 the oxidation of chloride anions to chlorine gas, P_3 the oxygen formation reaction, P_4 the reduction of chlorine gas back to chloride ions, P_5 the reduction of elemental sulphur to sulphide ions and P_6 the hydrogen forming reaction.

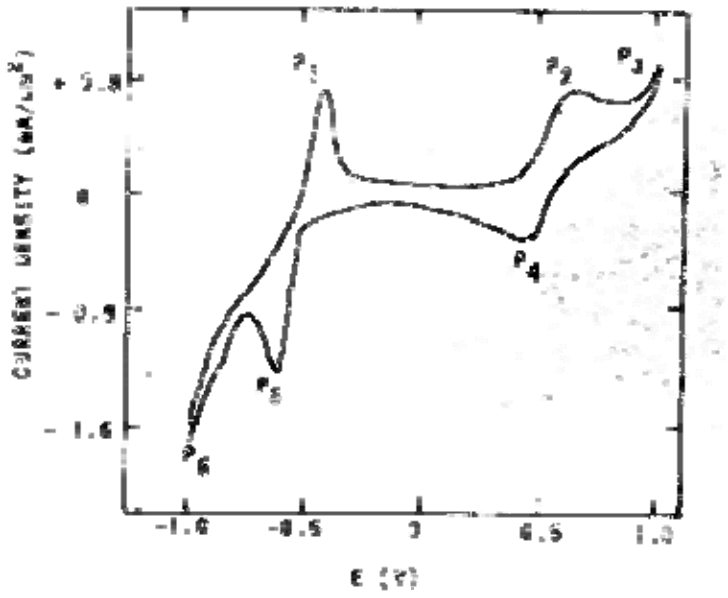

Figure 5. A cyclic voltammogram on 20 % sphalerite-carbon-paste electrode in 1M HCl at 60℃, with scan rate 100 mV/s. [43]

Pesonen [35] applied electrochemical methods to study the dissolution of sulphide minerals. It was found that increased temperatures and potentials accelerated the dissolution process, as is to be expected. Methods used were anodic polarisation, cyclic voltammetry and potentiostatic dissolution. A graphite paste electrode was used as a sample holder for the powdered sulphides, forming the working electrode. The graphite paste was found to be practically inert in electrochemical

measurements. This has been corroborated by Ahlberg *et al*. [22] in their electrochemical study of sphalerite. However, Crundwell [18] discussed studies which show the contrary: the mechanism of sphalerite dissolution was changed by the presence of graphite.

An electrode material has to be sufficiently conductive. Zinc sulphide, which has a high ohmic resistance, has to be blended with a conductive matrix before it is made into an electrode. Conducting sulphide mattes containing Co and Fe, as well as graphite-ZnS pastes, have been used to study electrochemical dissolution reactions. [44] Graphite and pitch containing compact electrodes, as well as carbon paste electrodes, were used by Srinivasan *et al*. [5] in cyclic voltammetric measurements of sphalerite.

5. CONDUCTIVITY AND ITS EFFECT ON DISSOLUTION

5.1 The band theory of crystalline solids

In free atoms, the energies of electrons are determined by the energy levels of the shells they occupy. As two atoms are brought closer together, the electron clouds partially overlap and the electrons are affected by both nuclei. Each of the previous energy levels is split into two new levels, as shown in figure 6. In a crystal consisting of *N* atoms, *N* linear combinations of atomic orbitals (LCAO) are formed from each preceding energy state. When a large number of atoms are participating, the differences between the separate discreet energy levels become very small and continuous energy bands are formed. The energy levels are divided between the valence band and the conduction band as shown in figure 6. [27]

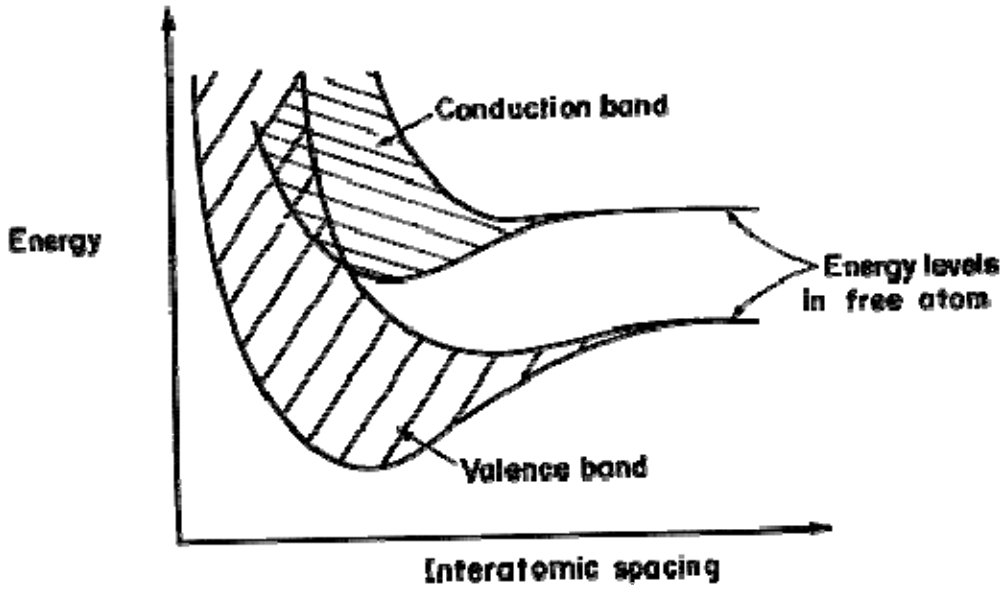

Figure 6. The splitting of energy levels and the energy band structure. [45]

If the orbitals forming the band are filled in the ground state of the separated atoms, the number of spin orbitals in the band equals the number of electrons in the band and the band is full, the electrons cannot move within the band. If the forming orbitals are only half full, also the band is only partially filled. The highest occupied band in the crystal is responsible for the conductive properties of

the material. If this band is full, electron transfer between orbitals cannot occur unless some of the orbitals can be vacated by moving some electrons to a band of higher energy. [27]

The degree of occupancy of each orbital is determined by the so-called Fermi level and the band gap associated with the molecule in question. The Fermi level is the value of the chemical potential of an electron. At 0 K all of the orbitals with energies up to the Fermi level are fully occupied and all of the orbitals above it are completely empty. At finite temperature, some of the electrons from the energy levels just below the Fermi level have enough energy to occupy some orbitals with energy just above the Fermi level. As temperature is increased more of the states under the Fermi level become unoccupied and more of the states above the Fermi level become occupied. [27]

The fermion probability distribution changes from approximately unity to nearly zero over a range of energy equal approximately to $k_B T$. In Figure 7 the fermion probability distribution is shown in terms of degenerate energy levels at 0K and at a finite temperature. The rising curve represents the number of degenerate energy levels and the lines T = 0 and T > 0 show the degree of occupancy of the energy levels at given temperatures. [27]

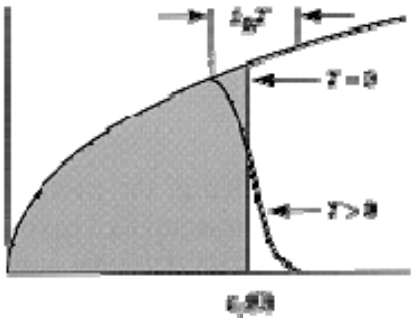

Figure 7. The degeneracy and the degree of occupancy of energy levels at 0 K and at a finite temperature. [27]

5.1.1 Electrical conductors

A crystal acts as an electrical conductor when the highest occupied energy band is roughly half full, since there are plenty of both electrons and unoccupied orbitals for them to move into. [27]

If the highest occupied band is full, the conductivity of the material is determined by the energy needed for an electron to move from the valence band into the conduction band. If the interatomic distance lies within the area where the bands are overlapping, as shown in figure 8, the material is a conductor. Some electrons from the full valence band can occupy and move through the orbitals of the conductance band, leaving free orbitals in the valence band for electron movement. For a conducting crystal the Fermi level lies within the band. The conductivities of typical metals are $10^4 – 10^6$ ohm^{-1} cm^{-1}. [27], [46]

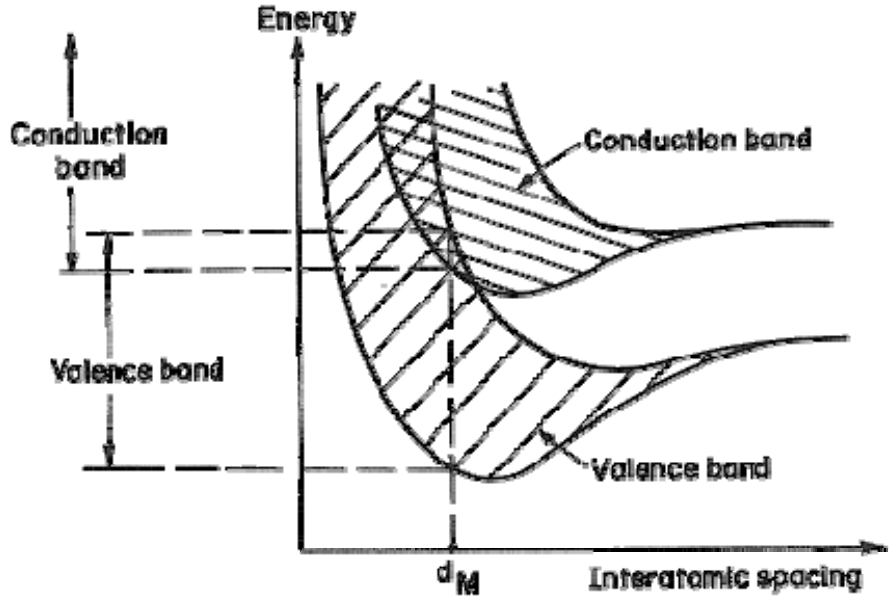

Figure 8. The band picture of a metal with an interatomic spacing of d_M, showing an overlap of the valence and conduction bands. [45]

5.1.2 Electrical insulators

A material is an insulator or a semiconductor if the highest occupied energy band is full and the interatomic distance lies within an area where the bands are separated by the band gap. The band gap is an area of forbidden energy levels between the conduction and valence bands as expressed in figure 9. In such a case the Fermi level lies between the two bands or at the top of the lower band. If the energy needed to move an electron from the valence band into the conduction band is far greater than the thermal energy of the electrons, the movement is highly improbable and the material is an insulator. The amount of thermal energy, k_BT, is not able to move a sufficient amount of electrons to the conduction band, and one band stays full and the other one empty. The conductivities of insulators are usually below 10^{-15} ohm^{-1} cm^{-1}. [46], [27]

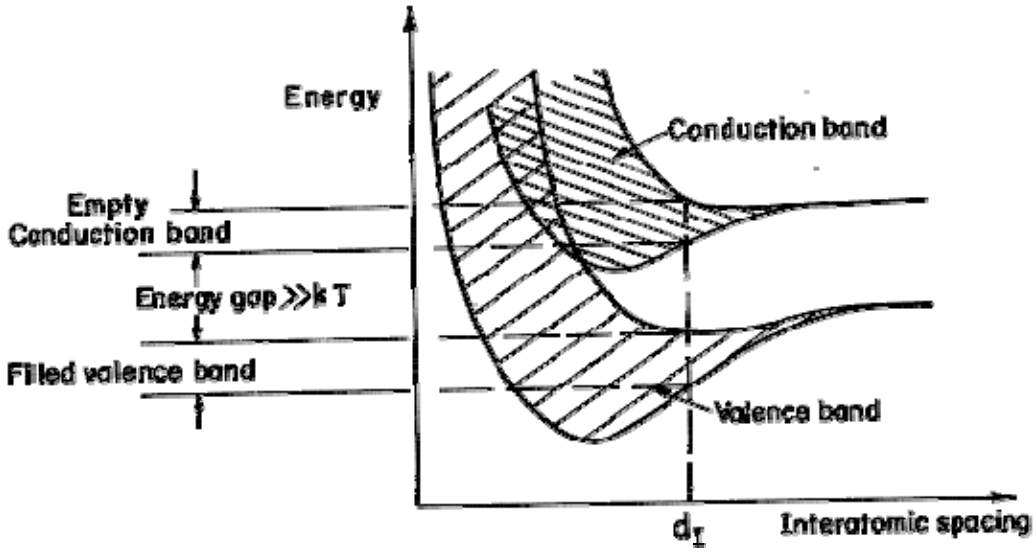

Figure 9. The band picture of an insulator with an interatomic spacing of d_I , showing the filled valence band separated from the empty conduction band by a large energy gap. [45]

5.1.3 Electrical semiconductors

There are two cases in which a crystal is a semiconductor when the highest occupied energy band is not full. Firstly, when the band is almost empty, there are plenty of empty orbitals to move into, but not many electrons to do so (*n*-type semiconductor). Secondly, when the band is almost full, there are enough electrons, but very few empty orbitals to move into (*p*-type semiconductor). [27]

Semiconductors have relatively small band gaps. At normal temperatures, when the highest occupied band is originally full, some of the highest energy orbitals in the filled band are vacant and some of the lowest energy orbitals in the next 'empty' band are occupied. The band gap is roughly of the size of k_BT, which allows thermal energy to excite some of the electrons to the conductance band, creating a slight movement of electrons in the conductance band and free orbitals in the valence band. This explains why the conductivity of semiconductors is very dependent on temperature: the higher the thermal energy, the more electrons can move to the conduction band. The band structure of a semiconductor is expressed in figure 10. The conductivities of semiconductors are typically 10^{-5} – 10^{3} ohm^{-1} cm^{-1}. [27], [39]

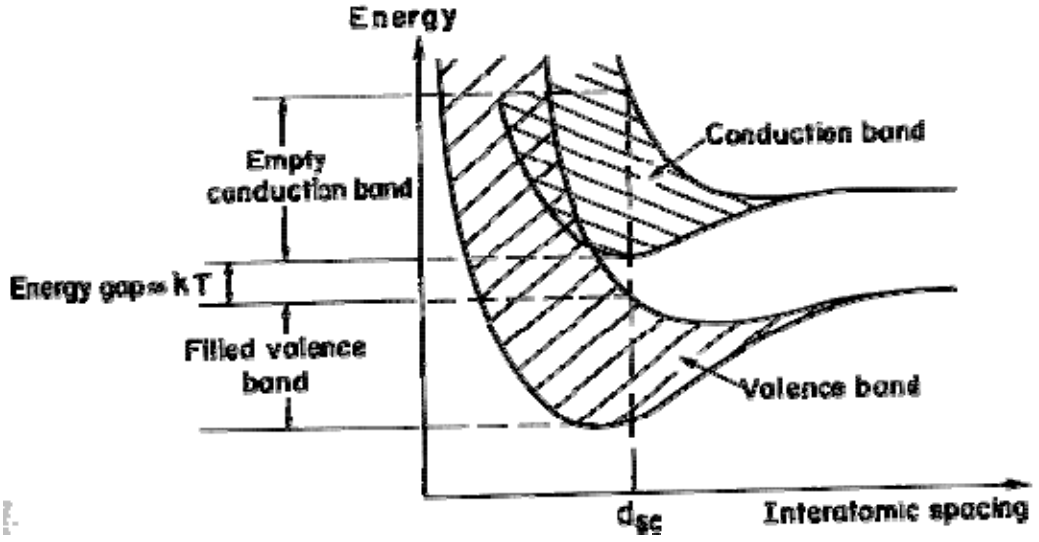

Figure 10. The band picture of a semiconductor with an interatomic spacing of d_{SC}, showing the energy gap between the valence and conduction bands. [45]

In intrinsic, natural semiconductors conductivity is based on the effects of thermal energy or radiation on the lattice. Heating allows electrons to be removed from atomic bonds, thus creating both a free electron and a free orbital, or a ‘hole’. Heating also gives sufficient energy for electrons to move over the band gap. In the photoelectric effect the electron is removed from the band by short wavelength radiation. The electron and the hole move in opposite directions in an external electric field and carry a current. At equilibrium, holes and electrons are formed at the same rate as they recombine and replace electrons in the atomic bond. [45]

In an intrinsic semiconductor the concentrations of holes and electrons are equal. This is true considering the whole of the conductor, but when discussing the surface layer in contact with an electrolyte, electric interactions have to be taken into account. From the electrolyte the outer Helmholz plane (OHP), which forms of ions electrostatically adsorbed on the semiconductor surface, exerts an electric field on the electrons and holes near the semiconductor surface. Similarly, a charged electrode exerts a field on ions in the electrolyte. Due to the field exerted on the semiconductor, electrons and holes are not present in equal concentrations near the surface. This charge imbalance is called the Garret-Brattain space charge. Using the Poisson-Bolzmann equation and the Gouy-Chapman diffuse-layer theory it can be shown that due to the space charge inside the semiconductor, there is an exponential decay of potential. The space charge and the changes in charge density and potential in a semiconductor/electrolyte system are shown in figure 11 on page 27. [45], [47]

This decay of potential implies the similarity of the semiconductor surface and the electric double layer in the electrolyte. An electric field extends to both and the excess-charge density inside the semiconductor, alike the ionic cloud in the solution, decays toward zero at distances away from the surface. Parameter κ used in the Debye-Huckel and Gouy-Chapman theories also describes the potential in the semiconductor surface layer caused by the space charge. Similarly, the thickness of the Garrett-Brattain space charge inside a semiconductor is expressed by κ^{-1}, the Debye length. This layer becomes thinner as the concentration of charge carriers increases throughout the semiconductor. When both ions in the

electrolyte and charge carriers in the electrode are abundant, the thickness of a charge layer formed by chemisorption can be only a few atoms.[45]

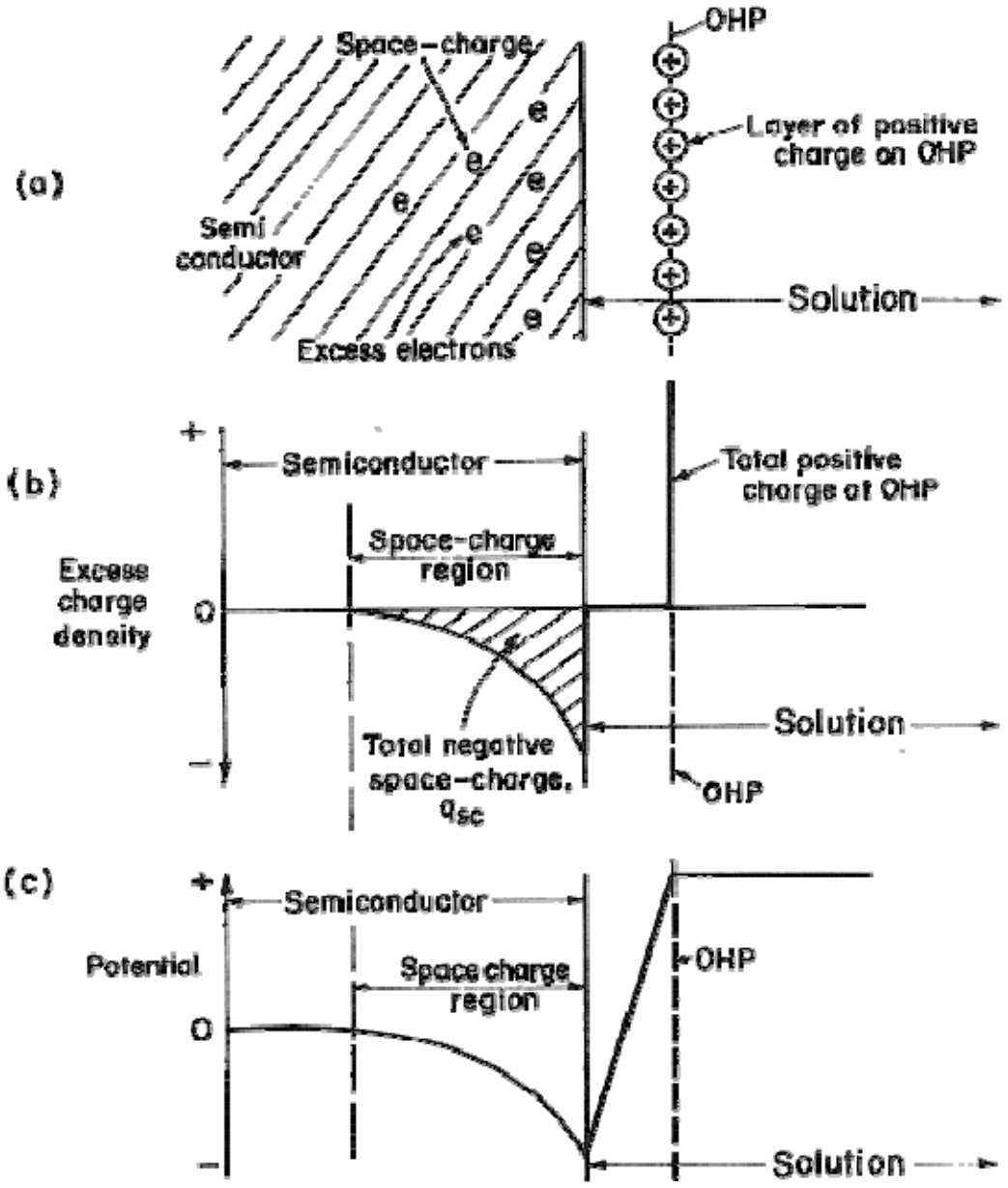

Figure 11. a) The space charge inside a semiconductor, b) the corresponding charge-density variation, and c) the potential variation. [45]

The energies of electrons in the bulk of a semiconductor are given by the band structure. The electrons in the Garrett-Brattain layer are affected by the electric field and the energies of the electrons are changed by this interaction. This can be seen in the band structure as bending of the bands near the semiconductor surface.

Positive charge on the outer Helmholz plane bends the bands to a lower energy level and a negative charge to a higher energy level. [45]

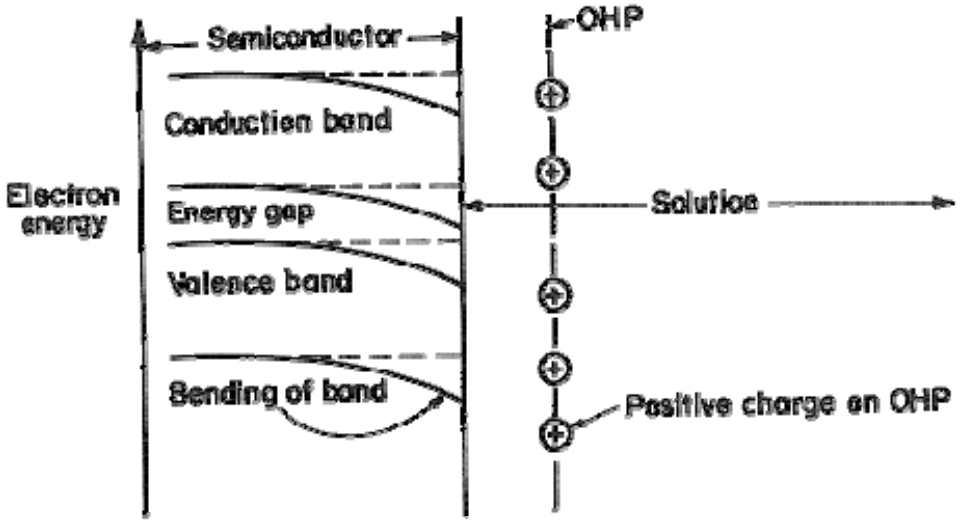

Figure 12. The bending of energy bands near a semiconductor surface. [45]

Three separate layers are formed near the boundary: a space charge layer of 100 – 10 000 Å within the semiconductor (the Garret-Brattain layer), a Helmholz double layer from the phase boundary a few atomic layers into the electrolyte, and the diffuse layer of the electrolyte (the Gouy-Chapman layer). The potential drop over a semiconductor/electrolyte interface is determined by the individual potential changes over these layers: the Garret-Brattain space-charge drop $\Delta\phi_{SC}$, the Helmholz-Perrin drop $\Delta\phi_{HP}$ and the Gouy-Chapman drop $\Delta\phi_{GC}$. [45], [47]

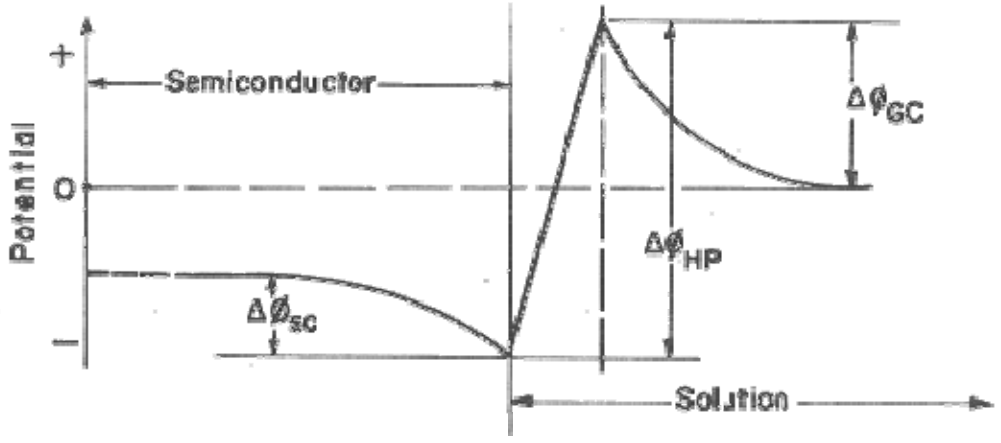

Figure 13. The potential variation at a semiconductor-electrolyte surface. [45]

There is one more effect to be taken into account when considering potential changes in the semiconductor/electrolyte interface. In this discussion so far, only charge carriers which are free to move in electric and thermal fields, have been considered. If electrons are bound in the surface energy states, as would be the case when atoms are adsorbed to the semiconductor surface, the Garrett-Brattain space-charge region is affected by these immobilized charges. Both, the potential drop across this layer and the charge associated with it, are reduced by surface states and approach zero, if the density of these states grows high enough. The potential in the semiconductor becomes uniform and charge is distributed mainly on the surface, in effect, the behaviour of the semiconductor approaches that of a metal. [39]

5.2 Effect of impurities and lattice defects

5.2.1 Doped semiconductors

Doped semiconductor conductivity is caused by the effect of impurities in the lattice. The impurity atoms can either donate electrons (*n*-type) or accept electrons (*p*-type). By doping a natural semiconductor with a donor, the electrons can be made to be the sole carrier of the current. Similarly, doping with acceptor atoms causes the current to be carried by the holes. [46]

The energy of the dopant atoms is in between those of the conduction and valence bands of the lattice. In *n*-type semiconductors, the energy of the dopant atoms is slightly lower than the energy of the conductance band. The electrons from the dopant can easily move to the conduction band, while the contribution from the valence band is minimal. In *p*-type semiconductors the electron energy of the acceptor atoms is slightly higher than the energy of the valence band. Electrons from the band can move to the acceptor atoms, leaving free orbitals in the band. These phenomena are described in figure 14 on page 30. [46]

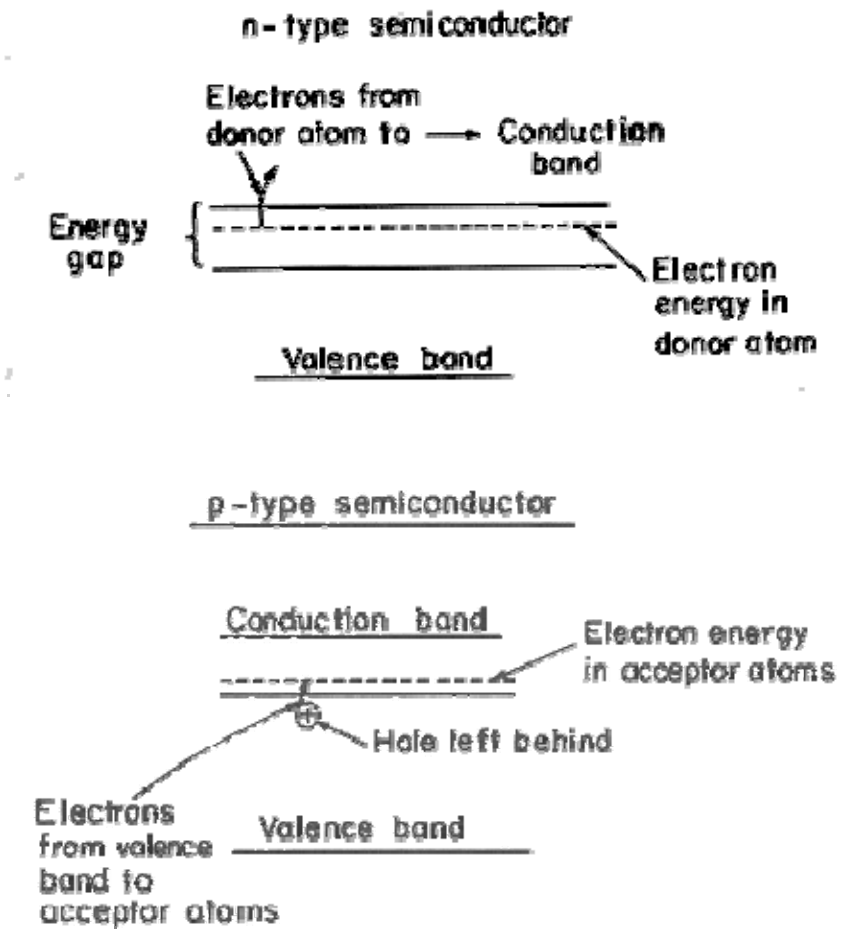

Figure 14. Band pictures of n-type and p-type semiconductors. [45]

Mikhlin *et al.* [48] found that the theory of surface passivation by elemental sulphur did not fit the results of their electrochemical studies of galena and sphalerite. They proposed that the formation and transformations of non-equilibrium metal-depleted layers (NL) are responsible for the leaching and electrochemical behaviour of the minerals. The NL include sulphur centres which act as dopants, causing the semi-conducting properties of the NL to become non-uniform. The centres also act as active surface centres and react with solution reagents. The transformations of these centres may be the main influence on the alterations of the surface layers. The characteristics of non-crystalline chalcogenide semiconductors are related to the lone pair *p*-orbitals of chalcogen atoms. Similarly the NL should be considered as a disordered semiconductor, with properties governed by negative correlation energy centres associated with sulphur atoms. The movement of charge carriers in a disordered semiconductor is

limited by being trapped in localised states, and the conductivity is low. Thus any heterogeneity has a significant effect on the properties of a disordered semiconductor.

5.2.2 Lattice defects

Defects in the lattice have a vast effect on the behaviour of any crystal. Vacancies, interstitial site atoms and substitutional atoms, as well as structural deformations, such as stacking defects and dislocations, affect the chemistry and properties of the substance. These primary defects can also combine to more complex deformations. Structural defects can in many cases be caused by temperature alone, but some are also formed during lattice growth and mechanical processing. Readily occuring interaction between lattice defects in ZnS makes the study of the separate effects difficult. [46]

Vacancies are formed when an atom is removed from its position in the lattice. A vacancy causes a local imbalance in the electrical equilibrium of the lattice, which has to be balanced by transferring electrons to or from the area of the vacancy: in effect vacancies act as donors or acceptors. A Schottky defect is a pair of vacant sites, as both an anion and a cation vacancy have been formed. A two-dimensional representation of a Schottky defect is pictured in figure 15. [46]

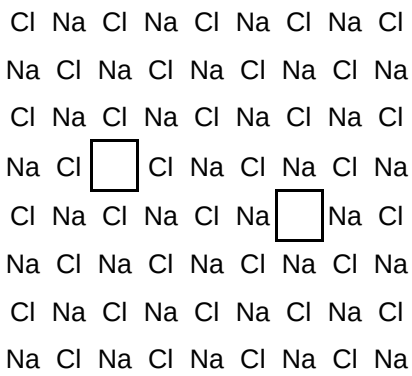

Figure 15. A two-dimensional representation of a Schottky defect in a NaCl crystal.

Interstitial sites are the places within the lattice that are usually unoccupied. When an ion from the lattice or from an impurity moves to an interstitial site, it acts as a donor if it is more electropositive than the surroundings, and as an acceptor when it is more electronegative. A Frenkel defect is formed when an atom in the lattice in displaced to an interstitial site as pictured in figure 16. [46]

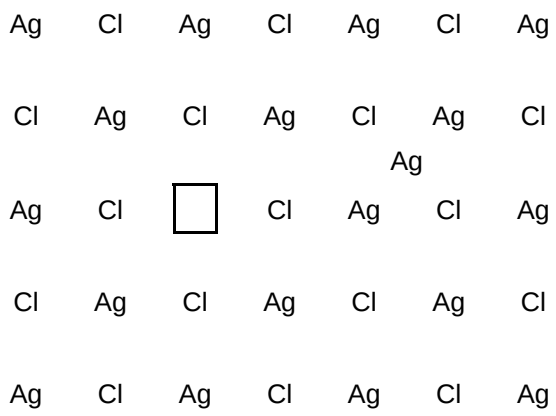

Figure 16. A two-dimentional representation of a Frenkel defect in a AgCl crystal.

Atoms which replace an original atom in the lattice are called substitutional atoms. They can be other atoms from the lattice or impurities from outside it. If the original and new atom have the same charge, the electrical balance is not changed, but replacement with an atom of differing charge causes the site to act as an acceptor or a donor. [49]

Point defects, such as Schottky defects, Frenkel defects and substitutional atoms, can be studied with thermodynamical methods, by applying the law of mass action to the equilibria. In most cases, the defects can be considered as an ideally dilute solution, with activity coefficients equal to unity. An alternate method is to use statistical thermodynamics to examine the lattice defects and their interactions. [45], [46]

5.2.3 Impurities

Impurities in metal sulphides are mostly present as substitutional atoms or ions, and have a great impact on the electric properties of the mineral. Metal cations are usually substituted by two or more different cations and sulphur can be substituted by arsenic or selenium. In a covalent semiconductor, substitution with an atom of lower valence forms an acceptor, a higher valence substitute forming a donor. [49]

The extent to which the donor or acceptor atoms ionise is determined by the Fermi level energy, E_f. For acceptor atoms, the degree of ionisation is given by

$$\frac{N_{a-}}{N_a} = \frac{½\exp((E_f - E_{ac})/k_B T)}{1 + ½\exp((E_f - E_{ac})/k_B T)} \tag{14}$$

where N_{a-} is the amount of ionised acceptor atoms, N_a is the amount of acceptor atoms, E_f is the Fermi level energy of the semiconductor, E_{ac} is the ionisation energy of the acceptor and k_B is the Bolzmann constant. [49]

E_{ac} and E_f are evaluated on the level of the top of the valence band. For donor atoms a similar equation applies:

$$\frac{N_{a-}}{N_a} = \frac{½\exp((E_d - E_f)/k_B T)}{1 + ½\exp((E_d - E_f)/k_B T)} \tag{15}$$

where E_d is the ionisation energy of the donor. [49]

At room temperature, the equilibrium constant for the formation of a Schottky defect in a ZnS lattice is large compared to the equilibrium constant of the electron and hole forming reaction. The shift from equilibrium caused by impurities is therefore compensated by the formation of vacancies, which keeps the amount of free charge carriers very small. The charge carriers are bound tightly to the lattice deformations and current cannot flow. However, if enough

iron atoms are present as impurities, the movement of holes between the iron atoms can create some current. [49]

Several pre-treatments have been studied to enhance the dissolution of sphalerite ores. Mechanical activation accelerates the rate of dissolution due to smaller particle size, larger surface area and formation of lattice defects, which increases the reactivity of the ore. UV-radiation increases the number of free electrons and holes, which increase the conductivity of the semiconductor and thus enhance dissolution. [3]

5.3 Electrochemistry of sulphide minerals

In the anodic dissolution of minerals, the rate-determining step can be diffusion in the solid or in the solution, conductivity in the solid or the heterogenous reaction taking place at the surface of the solid. The effect of mineralogical factors is minimal if the dissolution rate is controlled by diffusion in the solution. The effect of impurities present is usually so great, that the type of the current carrying species and the nonstoichiometry of the mineral are of little importance to the rate of reaction. [49]

Holes act as charge carriers in anodic dissolution and electrons carry the charge in cathodic dissolution. Their concentration on the surface of the semiconductor determines the rate of electrochemical dissolution as can be seen from equations (16) and (17). The anodic limiting current is caused by the zero concentration of holes on the valence band, and the cathodic limiting current by the zero concentration of electrons on the conductance band. [49]

$$I_p = I_{p0}\left(\frac{p_s}{p_{s0}} - 1\right) \tag{16}$$

$$I_n = I_{n0}\left(1 - \frac{n_s}{n_{s0}}\right) \tag{17}$$

where p indicates a hole, n indicates an electron, I_p and I_n are the anodic and cathodic currents, I_{p0} and I_{n0} are the exchange currents, p_s and n_s are the concentrations of charge carriers on the surface and p_{s0} and n_{s0} are the equilibrium concentrations of charge carriers on the surface.

The basis of sulphide mineral and sulphur chemistry in direct leaching are represented in a study by Peters [50] published in 1976. Later studies have shown that the dissolution of metal sulphides in acidic conditions begins with the dissolution of the metal from the lattice, leaving a sulphide surface layer partly depleted by metal. This nonstoichiometric layer can undergo further metal dissolution or it can reconstruct, forming again a stoichiometric sulphide and precipitating elemental sulphur on the surface. [34] The sulphur in the sulphide can be oxidised to sulphate if the oxidation potential is high enough. As the metal content of the surface decreases, the properties shift from those of an *n*-type semiconductor to those of a *p*-type semiconductor, and the equilibrium potential of the sample is increased. [48] Due to this effect, larger anodic potentials are needed for the sample to continue dissolving. In effect, the insoluble product layer increases the resistivity of the surface layer. A greater overpotential is needed to dissolve the sulphur overstoichiometric layer. When the product layer is of elemental sulphur, which is electrochemically practically inert, the dissolution of the mineral continues under this layer. In such a case, the transport of electrons and the diffusion of ions through the sulphur layer can limit the rate of the reaction [34].

At lower temperatures, an elemental sulphur layer does not immediately block the surface of the particle. At higher temperatures the problem is more immediate, as sulphur melts at 119°C and covers mineral particles as a compact layer causing the dissolution to stop. This can be prevented by the use of surface-active substances, such as lignosulfonate or quobracho, which cause the sulphur to form droplets on the surface, instead of spreading out over the whole surface area [28]. Lochmann *et al.* [20] found that the use of 1 g/l lignosulfonate in sphalerite leaching solution increased conversion from 30% to 60% after 3 hours by transforming the surface sulphur into porous form. Owusu *at al.* [51] studied the

effects of orthophenylene diamine (ODP), lignin sulphonic acid and metaphenylene diamine (MPD) as dispersants of liquid sulphur and found that conversion increased from 50% in 1 hour to > 99%, 86-94% and 95-98% respectively. Sulphur in its elemental form is very hydrofobic, while further oxidised sulphur species are of hydrophilic nature [49]. Speciation and quantification of elemental sulphur on mineral surfaces is discussed in an article by Toniazzo *et al*. [52].

The band structures of sulphides explain some of their properties. The electronic structure of the cation has been related the conductance band, the anion structure to the valence band. Transition metals also hold a band formed by the *d* electrons, which can add to the contribution from the cation to the valence band. [44]

Germanium has most commonly been used to study the electrochemistry of semiconductors, while CdS, an *n*-type semiconductor with a band gap of 2.4 eV, is the most studied sulphide. Its dissolution reaction is

$$CdS \rightarrow Cd^{2+} + S + 2e^{-} \qquad \text{(R8)}$$

and the mechanism suggested is based on the band theory of ionic crystals: A cadmium ion moves from the lattice to the surrounding solution, leaving excess electrons on the valence band. These electrons are unable to move since the valence band is full and they have to be moved to the conductance band before they can move into the external circuit. The energy needed to move the electrons over the band gap is provided by illumination. Thermal energy is sufficient for this movement in sulphides with smaller band gaps like FeS_2 or PbS. [44]

Specific adsorption of ions or lattice defects form energy levels between the conductance and valence bands, and it is shown that the electrocatalytic activity of CdS toward the redox couple Fe^{2+}/Fe^{3+} depends on the formation of these surface-states. Specific adsorption has been shown to take place on ZnS and PbS surfaces and the occurrence of an isoelectric point at *p*H 4 suggested the adsorbed species to be protons or hydroxyl ions. [44]

6. ZINC SULPHIDE

6.1 Structure

Zinc sulphide has two crystallographic forms, sphalerite and wurtzite. Sphalerite is stable at lower temperatures, wurtzite at higher temperatures. The lattice structure of sphalerite is cubic and the zinc atoms form a face centred lattice. The eight zinc atoms in a lattice cell form regular tetrahedrons in which the four sulphur atoms are situated. The bonds in wurtzite are alike those in sphalerite, but the tetrahedrons are differently arranged forming a hexagonal structure. Zinc blend is a mixture of these two structures, with the cubic form dominating. In an ionic model, the ions present are Zn^{2+} and S^{2-} regardless of the lattice structure. [26]

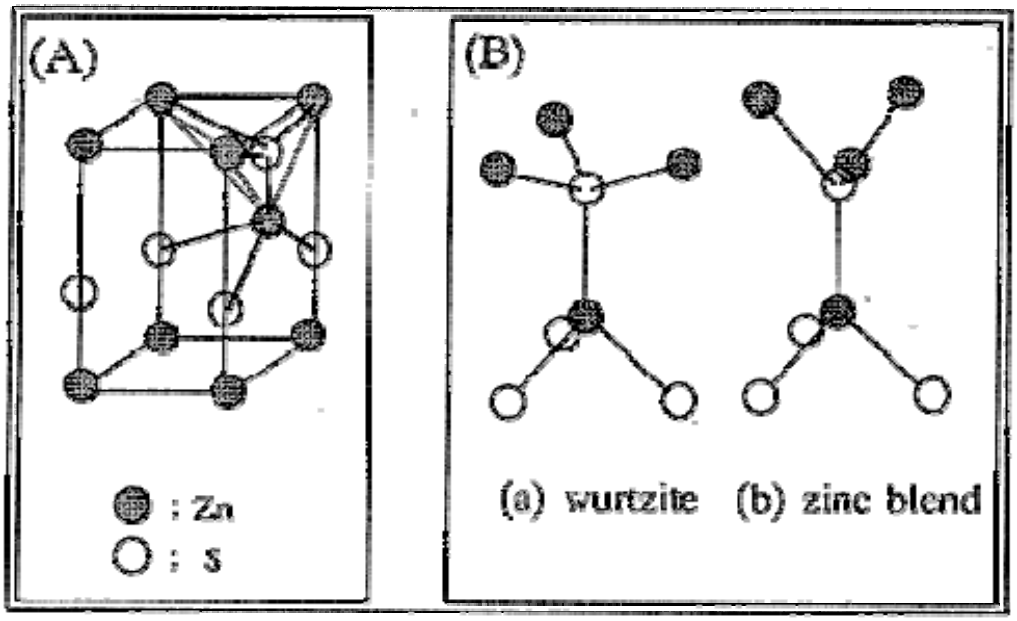

Figure 17. The crystal structure of zinc sulphide. A) A tetrahedron atomic arrangement B) The forms of ZnS: a) wurtzite and b) sphalerite. [26]

Nonstoichiometry occurs in both forms of ZnS, with excess ions in interstitial sites. Sphalerite has excess metal ions, forming an *n*-type semiconductor, while wurtzite is a *p*-type semiconductor with excess sulphur. A zinc ion in the lattice can be substituted by a Fe, Mg or Cd ion, increasing reactivity. The bonds in ZnS

are of covalent and ionic nature. Pauling has estimated that the Zn-S bond is 20 % ionic. In solid structures neither of these bonds conduct electricity, the semiconductor property being caused by the narrow band gap in a covalent bond crystal or by impurities. Iron is more electropositive than zinc, thus the presence of Fe-ions in sphalerite increases the ionic properties of the bond and therefore the rate of dissolution is also increased. [3], [26]

6.2 Electrochemical properties

The conductivity of pure ZnS is low, usually 10^{-11}-10^{-14} $\Omega^{-1}m^{-1}$ and the band gap for ZnS is usually large, 3.6-3.9 eV [3], [18], [22]. This makes the conductivity of sphalerite very dependent on the effects of impurities and temperature. The band gap can be narrowed greatly by substitutional atoms in the lattice: a 12.4 % iron content has been found to decrease the band gap of sphalerite to 0.5 eV. [22]

In the band model, the 4s orbital of Zn is associated with the bottom of the conduction band and the 3p orbital of sulphur with the top of the valence band. The d orbital of an iron impurity atom gives rise to an additional conducting band. Iron impurity induced localised bands have been reported to have energies 0.56 eV and 1.44 eV above the valence band. The Fermi level, expressing the electrochemical potential of the semiconductor electrons, is ‘pinned down’ by the presence of the iron *d* orbitals. [42]

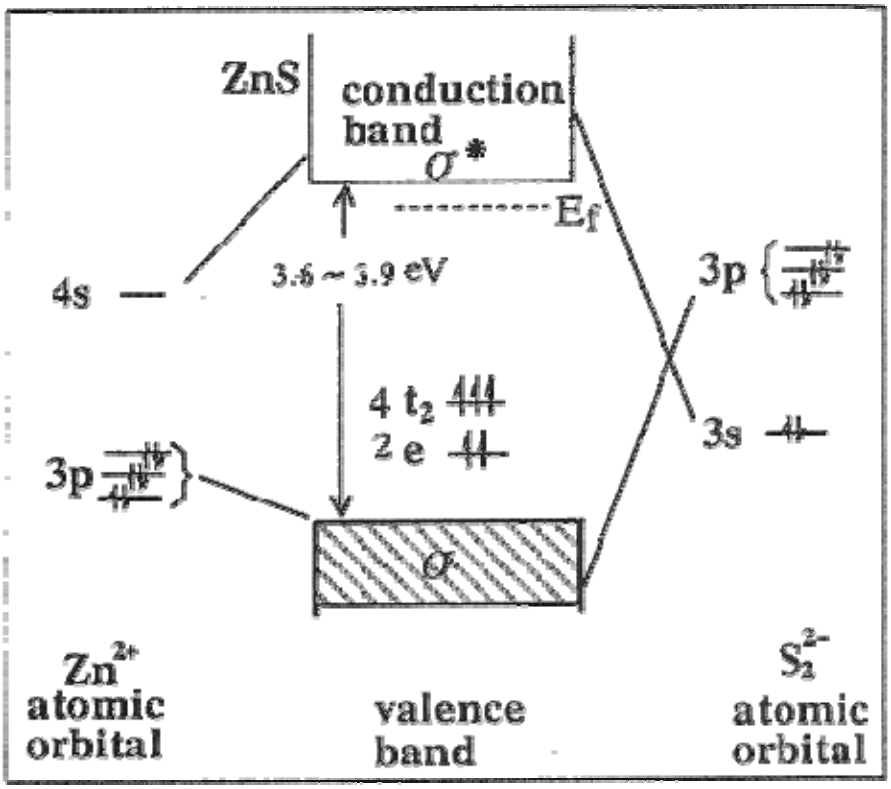

Figure 18. The band structure of ZnS. The t_2 and e levels represent the effect of iron impurities. [26]

7 ELECTROCHEMICAL METHODS FOR THE STUDY OF DISSOLUTION KINETICS

7.1 The dependence of solution potential on the ferric / ferrous ion ratio

In atmospheric dissolution of sphalerite concentrate, ferric ions are used as the oxidising agent. For each mole of zinc dissolved two moles of ferric ions reduce to ferrous ions according to (R1). Oxygen is fed to leaching reactors to oxidise the formed ferrous ions back to the ferric form, in order to enable further dissolution. In an oxygen-free environment, the dissolution of ZnS causes for the ferric/ferrous -ion ratio to change and the accumulation of ferrous ions is directly proportional to the extent of dissolution.

The ratio of ferric to ferrous ions in solution can be studied by measuring the potential of the solution with a platinum electrode with a Ag/AgCl –electrode as the reference. As the Fe^{3+}/Fe^{2+} -ratio decreases, so does the potential difference between the two electrodes. By measuring the potentials of solutions with a known Fe^{3+}/Fe^{2+} -ratio it is possible to produce a calibration curve, which enables the constant monitoring of the degree of dissolution. A calibration curve of potential versus Fe^{3+} mole fraction is shown in figure 19.

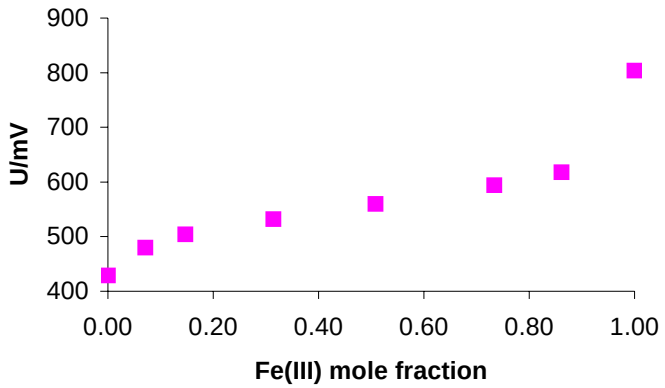

Figure 19. Potential as a function of Fe^{3+} mole fraction in 2.2 M H_2SO_4 at 90 ℃.

As can be seen, the dependence is quite linear between the Fe^{3+} mole fractions 0.15 and 0.85. Naturally, the end points, mole fractions 0 and 1, are not exact points of measurement, since the platinum electrode is sensitive only to the ratio of the two ions. Both ions are always present to some extent due to thermodynamical necessity and the end points merely show the direction of change.

7.2 Scanning electrochemical microscopy

Scanning electrochemical microscopy (SECM) is a scanning probe technique in which the current caused by an electrochemical reaction is measured. When the electrode approaches a surface, the changes in current can be used to identify redox reactions taking place at the surface and to calculate the rates of these reactions. The measurement set up is depicted in figure 20. [53]

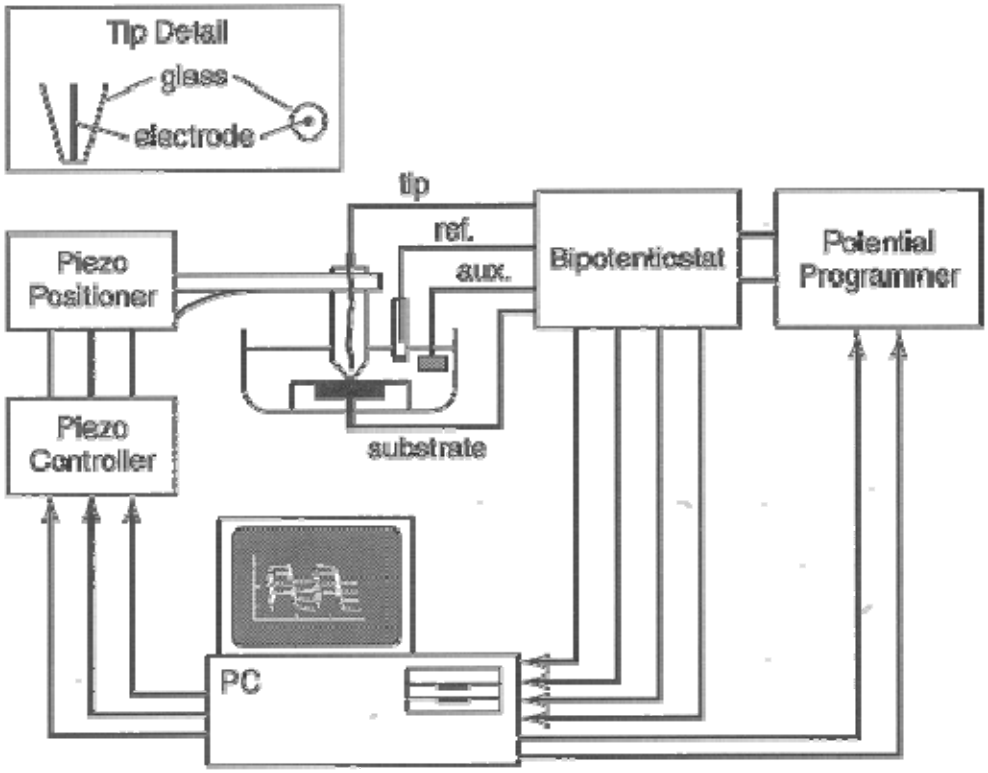

Figure 20. A schematic diagram of SECM apparatus. [53]

The measurement cell consists of an electrode tip, reference and auxiliary electrodes and the sample, which are all connected to a bipotentiostat. The electrode tip is commonly a platinum or carbon disc of 1-25µm radius, sealed in glass and it is moved by piezo controllers. [53]

The tip and the sample are immersed in an electrolyte solution containing an electroactive substance and placed some distance away from each other. A potential is then applied, and an electrochemical reaction between the electrode tip and the electroactive species takes place, causing a steady-state current $I_{T,\infty}$:

$$I_{T,\infty} = 4nFD_oC_o^*a \tag{18}$$

where D_o is the diffusion coefficient of the electroactive species, C_o^* is the bulk concentration of the electroactive species and a is the radius of the electrode tip. [53]

The tip is moved closer to the sample and at a distance of a few tip radii, a change in the current is detected. The current is decreased as the sample surface inhibits diffusion of the electroactive species to the electrode tip. However, if the sample can take part in the redox cycle by oxidising the species reduced by the electrode, the current is increased as expressed in figure 21 on page 43.

Approach curves can be used to study the rates of heterogenous redox reactions at the sample surface and voltammograms give information on the rates of heterogenous electron transfer. [53]

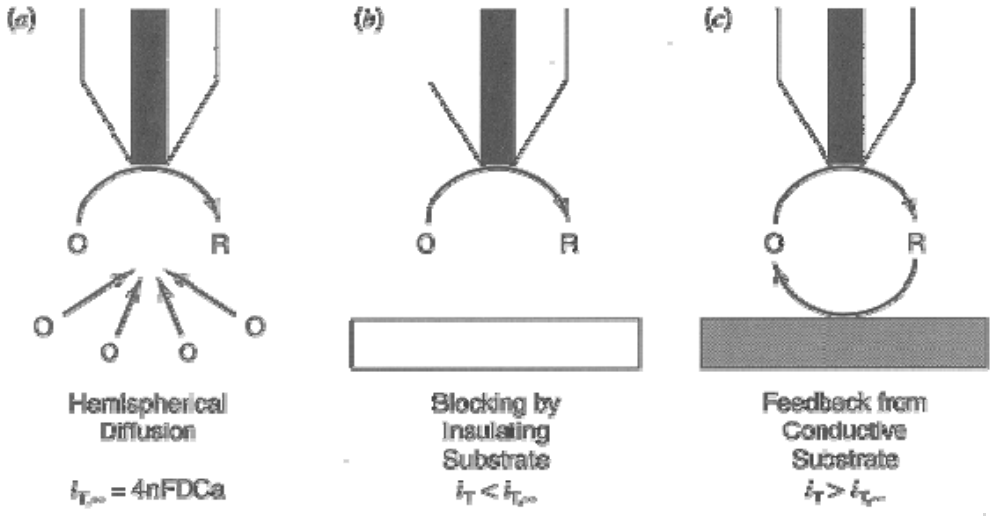

Figure 21. Principles of SECM, showing (a) hemispherical diffusion to the disc-shaped tip far from substrate, (b) blocking of diffusion by insulating substrate, (c) positive feedback at a conductive substrate. [53]

8 EXPERIMENTAL

8.1 Introduction

One objective of this study was to establish an *in-situ* method for monitoring the dissolution of sphalerite concentrates in sulphuric acid with ferric sulphate. A method based on monitoring the solution's electrochemical potential was studied and dissolution experiments were conducted to examine the applicability of this method. The change in Fe^{3+} to Fe^{2+} ratio in the solution was measured as a function of time with a platinum electrode, and the conversion of zinc sulphide to zinc ions was calculated from these results. To evaluate the accuracy of this method, solution samples were analysed with AAS and concurrent conversions were calculated.

Another purpose of these experiments was to study how different process variables affect the rate of this dissolution process. The variables in the measurements were particle size, temperature, rate of stirring and the concentrations of iron and zinc in the solution. The concentration of sulphuric acid was kept uniform and all experiments were conducted under atmospheric pressure in oxygen-free solutions.

8.2 Chemicals

All solutions were made with MilliPore ion-exchanged distilled water. Other chemicals used are presented in table 1.

Table 1. Chemicals used.

Chemical	**Grade**	**Manufacturer**
H_2SO_4 (l)	95-97 %	Merck
$Fe_2(SO_4)_3 \cdot x\ H_2O$ (s)	p.a.	Riedel-de Haën
$FeSO_4 \cdot 7\ H_2O$ (s)	p.a.	Riedel-de Haën
$ZnSO_4 \cdot 7\ H_2O$ (s)	p.a.	Riedel-de Haën
N_2 (g)	99.5 %	Oy Aga Ab

To determine the amount of crystalline water in the iron-(III)-sulphate used, a thermometric analysis of the powder was conducted, as well as an AAS-analysis of the sulphate in an aqueous sulphuric acid solution. The thermometric analysis gave the substance a molar mass of 510 g/mol, while the molar mass calculated from the AAS analysis was 580 g/mol. One possible reason for this discrepancy is partial dissolution of the sulphate in the solvent. If all of the sulphate was not dissociated, the effective iron-(III) content in the solution would be less than intended. Since the molar masses calculated from various different AAS analysis were all substantially closer to 580 g/mol than 510 g/mol, the former value was used for calculating the effective iron content in the solution.

8.3 Concentrates

Four different size fractions of a single Outokumpu Pyhäsalmi concentrate were studied. The chemical composition of the concentrate is expressed in figure 22 and the size fractions and surface areas in table 2. The concentrate was dried in a nitrogen atmosphere before it was divided to fractions and the surface areas were measured using the BET-technique with nitrogen as the adsorbant.

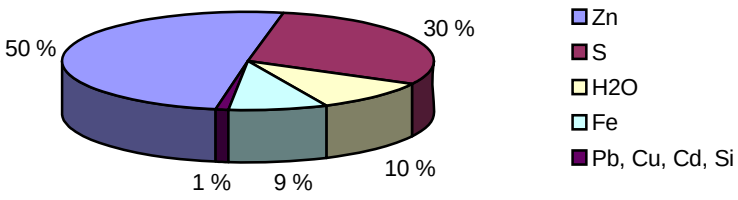

Figure 22. Chemical composition of concentrates studied.

Table 2. The size ranges and surface areas of the different concentrate fractions.

Fraction	**Size range**	**Surface area**
I	>105 µm	0.142 m^2/g
II	54 µm -105 µm	0.238 m^2/g
III	37 µm – 54 µm	0.377 m^2/g
IV	< 37 µm	1.220 m^2/g

8.3 Equipment and procedure

8.3.1 Apparatus

The dissolution experiments were conducted in a round-bottomed glass reactor of approximately 2 l volume. The Teflon cover had inlets for a reflux condenser, a stirring rod, a thermosensor, a gas tube and two electrodes. The stirring rod had four sets of four angled blades, and four stainless steel bafflers of 1.5 cm width were placed inside the reactor to ensure thorough stirring.

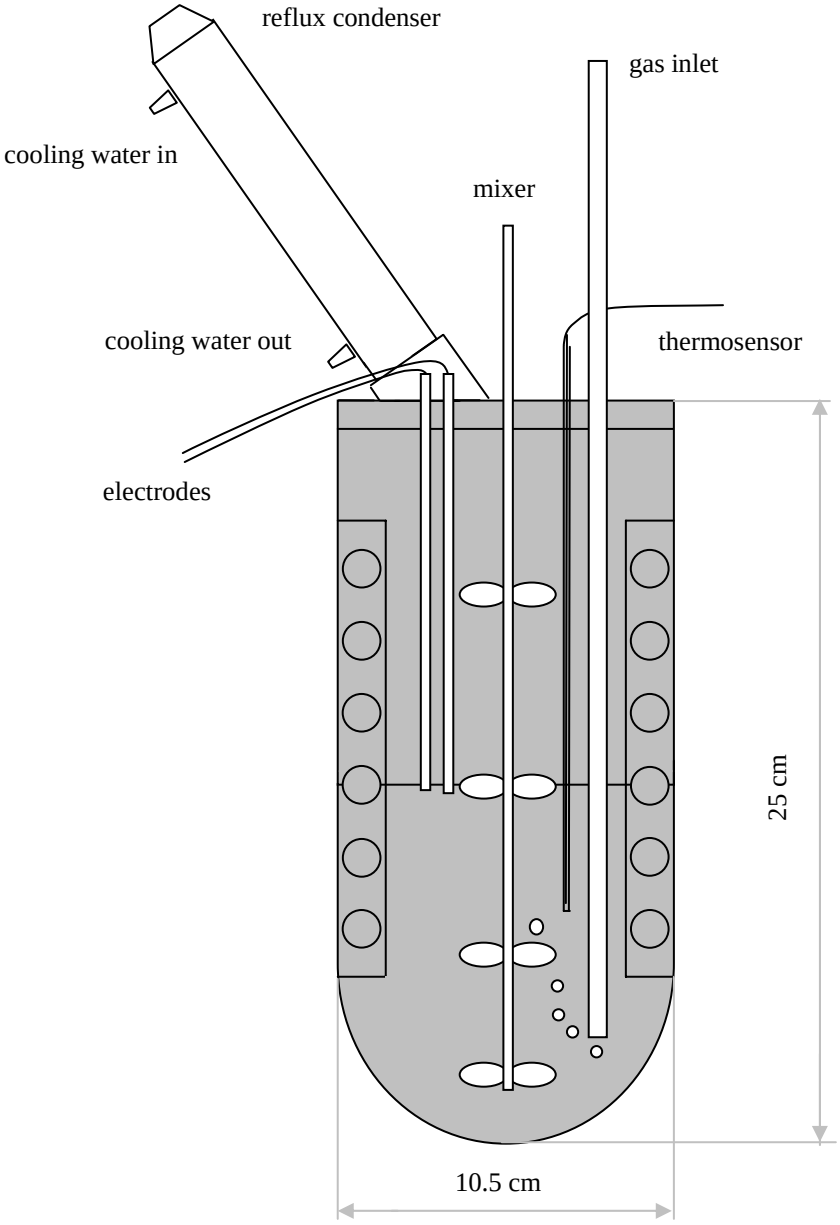

Figure 23. Schematic picture of the reaction vessel.

The chosen temperature was maintained by a flexible electric heating cover, which was placed around the vessel. The 200 cm × 300 cm cover was manufactured by Oy Meyer Vastus Ab, and it had a wattage of 300 W. A thermosensor was set in a glass tube partially filled with graphite oil and placed inside the reaction vessel. The thermosensor was connected to the heating cover though a controlling appliance, which adjusted the heating power of the cover according to the chosen temperature and the thermosensor signal. A picture of the apparatus is in appendix 1.

The platinum electrode was of platinum rod, 0.7 mm in diameter and 14 cm in length. The reference electrode was a commercial Ag/AgCl reference electrode, with a porous pin junction and a KCl salt bridge, type REF 201 from Radiometer analytical S. A. All potentials are given against the Ag/AgCl electrode.

8.3.2 Measurements

Sulphuric acid (0.2 M or 20g/l) was used in all measurements, the reactor filled up to 1.2 l or 1.5 l depending on the measurement. The acid was preheated and poured into the reaction vessel, where iron-(III)-sulphate was added. Nitrogen was bubbled through the solution for 15 minutes prior to measurement to remove the dissolved oxygen. In experiments M12-M20 nitrogen was fed continuously to ensure an oxygen-free environment. After oxygen had been removed and the temperature of the solution had stabilised, zinc concentrate was added to the solution (2 g/l). The solution was stirred at 1000 rpm in all experiments except M16 where the effect of stirring rate was studied. The conditions for each measurement are listed in table 3 on page 48.

In industrial process conditions, the process fluid is recycled and the solvent contains 100-150 g/l of dissolved zinc. In experiments M17-M20 100 g/l of Zn^{2+} was added to the warm sulphuric acid as the sulphate heptahydrate, prior to the addition of the iron-(III)-sulphate.

Table 3. Measurement conditions.

Measurement	***c*(Fe^{3+})/mM**	***T*/°C**	***V*/dm^3**	**fraction**	**other**
M1	52	60	1.2	II	N_2 only prior to measurement
M2	52	70	1.2	II	N_2 only prior to measurement
M3	52	80	1.2	II	N_2 only prior to measurement
M4	52	90	1.2	II	N_2 only prior to measurement
M5	75	80	1.5	I	N_2 only prior to measurement
M6	75	80	1.5	II	N_2 only prior to measurement
M7	75	80	1.5	III	N_2 only prior to measurement
M8	75	80	1.5	IV	N_2 only prior to measurement
M9	75	60	1.5	II	N_2 only prior to measurement
M10	75	70	1.5	II	N_2 only prior to measurement
M11	75	90	1.5	II	N_2 only prior to measurement
M12	33	60	1.5	II	
M13	33	70	1.5	II	
M14	33	80	1.5	II	
M15	33	90	1.5	II	
M16	75	80	1.5	II	mixing 500 rpm
M17	75	60	1.2	II	100 g/l Zn^{2+} in solution
M18	75	70	1.2	II	100 g/l Zn^{2+} in solution
M19	75	80	1.2	II	100 g/l Zn^{2+} in solution
M20	75	90	1.2	II	100 g/l Zn^{2+} in solution

The amount of zinc concentrate was 2 g/l in all measurements, which equals approximately 15 mmol/l. The different amounts of Fe^{3+} in the solution in the beginning of the experiments are listed in table 4, as are the concentrations, the ratios of iron to zinc concentrations and the iron overstoichiometry factors.

Table 4. Amounts of iron in the solution and the ratios of iron-(III) to zinc ions.

***m*(Fe^{3+})/(g/l)**	***c*(Fe^{3+})/(mmol/l)**	***c*(Fe^{3+})/*c*(Zn^{2+})**	**Fe^{3+} overstoichiometry**
10	33	2.2	1.1
15	52	3.5	1.75
22	75	4.8	2.4

During the measurements, the stirring was stopped for about one minute prior to taking samples for analysis. This allowed for the solids to settle at the bottom of the vessel, so a clear sample of the solution could be taken. The samples were taken with a glass pipette through the reflux condenser inlet in the Teflon cover.

For the analysis of the measured potentials, calibration curves were plotted. Four solutions with different ferric to ferrous ion ratios were made, using iron-(II)-sulphate and iron-(III)-sulphate. The total iron content in the solutions was equal to that in the actual measurements. In measurements M12-M15 the volume of the calibration solutions was 1.5 l, in all others a volume of 0.2 l was used. Nitrogen was bubbled through the solutions prior to the dissolution of iron-(II)-sulphate, in order to ensure that dissolved oxygen did not affect the ferric/ferrous ion equilibrium. The calibration solutions were heated to measurement temperature, and the potentials were measured. The ferric to ferrous ion ratios were plotted as a function of potential, four measured points forming each curve. By applying a function fitted to the calibration points, ferrous ion concentrations in the solutions were calculated. As all ferrous ion formation was accounted to the dissolution of zinc, conversions of zinc sulphide to dissolved zinc could be calculated.

8.3.3 Analysis

A 5 ml sample was taken from the solution at 0, 10, 20, 30, 40, 50, 60, 90, 120, 180, 240, 300 and 360 minutes from the addition of the concentrate. The zinc and iron concentrations in the sample were measured with atomic absorption spectrometry and the conversion of zinc at each time was calculated from this data. The ferric/ferrous ion ratio was measured by following the change in the potential between the platinum electrode and the reference electrode. The potential was recorded as each sample was taken. Conversions were also calculated from these potentials, using the assumption that the formation of Fe^{2+} is directly proportional to the amount of zinc dissolved.

In measurements M17-M20, the amount of dissolved zinc could not be analysed from the solution, due to the 100 g/l of Zn^{2+} in the solution. In these

measurements the undissolved residues were filtered from the solution, washed with distilled water and dried in a vacuum oven at 40°C for 5 hours. A part of these residues were then dissolved and analysed for zinc. The amount of sulphur in the residues was also analysed, using an IR-absorption Leco sulphur and carbon analyser. This was done in order to determine whether elemental sulphur had been oxidized to sulphate and thus dissolved. This would cause an error in the calculations, in which all Fe^{2+} formation had been accounted to the oxidation of sulphide to elemental sulphur.

9 RESULTS AND DISCUSSION

9.1 The correlation between potential and conversion

For measurements M1-M16, conversion was calculated both from the AAS analysis results and the measured potentials. Figure 24 shows an example of how the two separately calculated conversions correlated with each other, the rest of the comparisons can be seen in appendix 2.

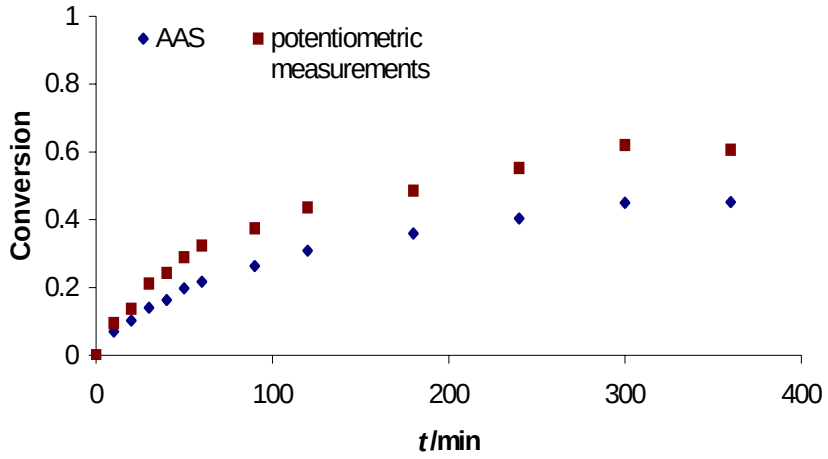

Figure 24. Correlation of conversions calculated from the AAS analysis results and the results of potentiometric measurements. Measurement carried out with concentrate fraction II, with an initial Fe^{3+} concentration of 33 mM, at 90 ℃.

Typically there is a 20 % difference in the conversions, although the two curves do correlate nicely in some measurements. The curves do usually have the same shape and the use of a correction factor, 0.7 in this case, gives a very good correlation, as can be seen in figure 25 on page 52.

The difference in the conversions could be caused by a systematic error in the calibration procedure. An alternative explanation could be the occurrence of another oxidation reaction, which would use up ferric ions and increase the amount of ferrous ions in the solution. Such a reaction is the oxidation of elemental sulphur to sulphate ions.

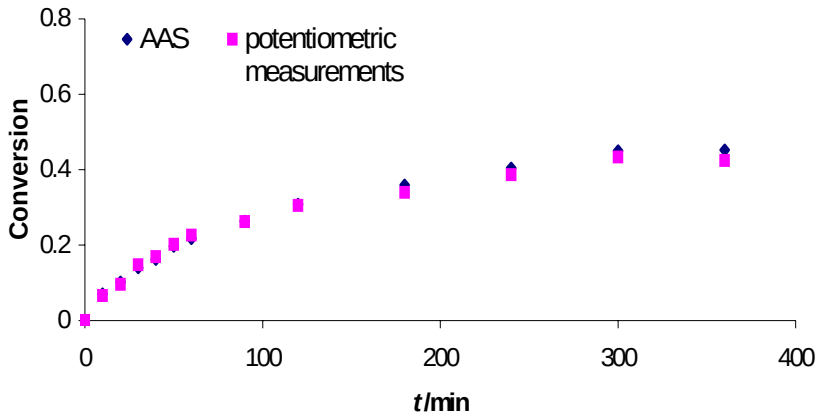

Figure 25. Correlation of conversions calculated from the AAS analysis results and the corrected results of potentiometric measurements. Measurement carried out with concentrate fraction II, with an initial Fe^{3+} concentration of 33 mM, at 90 °C.

In order to explore the possibility of a sulphate forming reaction, the sulphur content of the residues from experiments M17-M20 were analysed. As solid elemental sulphur is oxidised to the sulphate ion, it moves into the solution and the amount of sulphur in the solid is decreased. If analysis of the residue would show the residue to be depleted in sulphur, it would imply the presence of a sulphate forming reaction. Unfortunately, due to an error in the analysis, the results of the sulphur analysis are too inaccurate to be of use. Further study will show whether the sulphate forming reaction accounts for the differences in the conversions or if some other factors are involved. If the difference is shown to be solely due to the dissolution of sulphur, it could be used to study the extent of this reaction.

9.2 The effect of temperature

The effect of temperature on the rate of dissolution was studied with 3 series of experiments at temperatures 60, 70, 80 and 90°C. The Fe^{3+} concentrations for the series were 33, 52 and 75 mmol/l and size fraction II of the concentrate was used in all experiments. Conversions at different temperatures as a function of time are

seen in figures 26, 27 and 28 for Fe^{3+} concentrations 33, 53 and 75 mmol/l respectively.

For the series with 33 mM Fe^{3+}, it can be seen that the difference in conversion at different temperatures is greatest during the first 2 hours of dissolution. As time passes, the difference grows smaller, with conversions nearly equal at the end of the experiment. This behaviour is explained by the theory of surface reaction being the rate-determining step in the beginning of dissolution. The rate of the surface reaction is strongly affected by temperature, thus the differences in conversion at different temperatures are clear. As conversion increases, the product layer on the particle surface grows, causing the effect of diffusion to become more prominent.

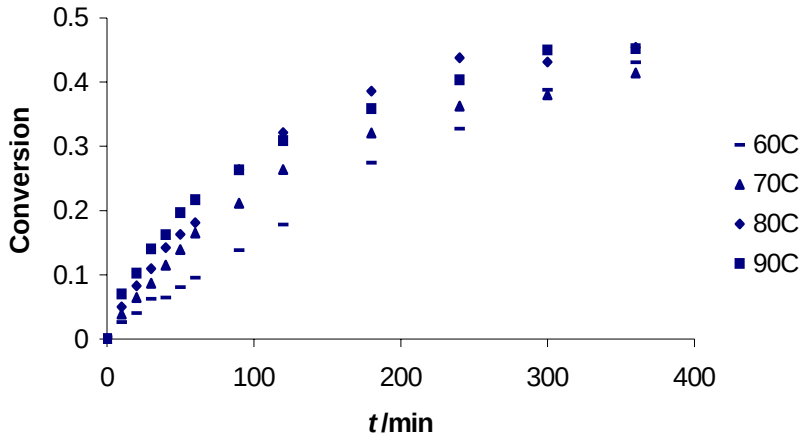

Figure 26. The effect of temperature on conversion. Measurements carried out with concentrate size fraction II and with 33 mM Fe in solution.

In this series, with 33 mM Fe^{3+}, ferric ion is present only in small overstoichiometry, and as dissolution advances, the concentration of ferric ions decreases, until diffusion of ferric ions to the particle surface becomes a considerable rate-limiting factor. As less and less ferric ions are present, the driving force of the diffusion is diminished and rate of dissolution is decreased. Due to this effect, the final conversions are almost equal for the measurements in different temperatures.

At ferric ion concentrations of 52 and 75 mM this effect is not seen, as more ferric ions remain in the solution at conversions reached. Diffusion of the ferric ions and dissolved zinc ions through the sulphur product layer eventually decrease the rate of dissolution. In both of these series the rate of dissolution was considerably lower for the experiment at 60 °C than for the three experiments conducted in higher temperatures. This would imply that the mechanism of dissolution changes as the temperature is increased.

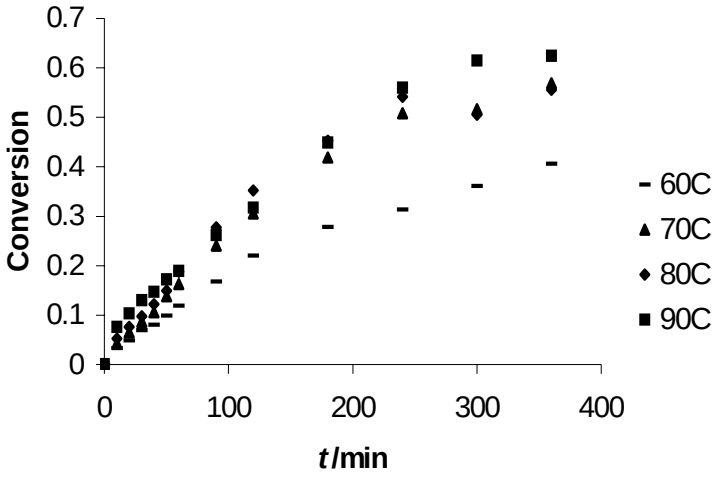

Figure 27. The effect of temperature on conversion. Measurements carried out with concentrate size fraction II and with 52 mM Fe in solution.

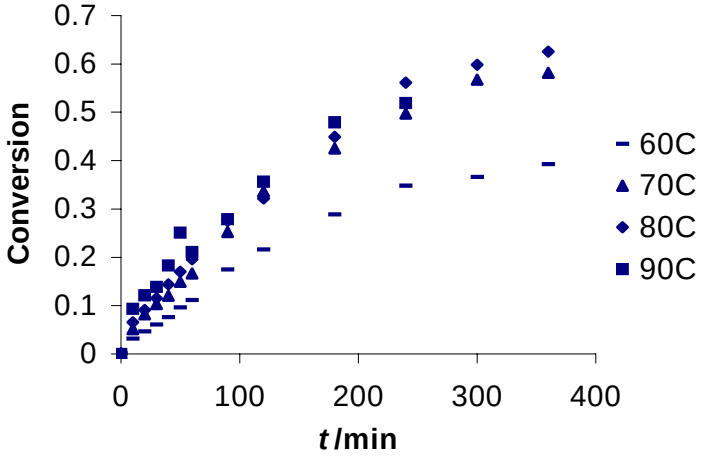

Figure 28. The effect of temperature on conversion. Measurements carried out with concentrate size fraction II and with 75 mM Fe in solution.

9.3 The effect of particle size

The effect of particle size was studied by conducting experiments on a different size fraction for each experiment, while all other parameters remained the same. The Fe^{3+} concentration in the beginning was 75 mM and the temperature was set at 80 °C. The conversions calculated from the analysed samples are presented as a function of time in figure 29.

Unsurprisingly, the rate of dissolution grew with the decrease of particle size. Comparing the two fractions of smallest particle size, III and IV, one can see that in the beginning of the measurement the rate of dissolution of fraction IV is considerably faster than the dissolution of fraction III. As time elapses, the difference in conversion is decreased and after four hours it is insignificant. The dissolution curve for fraction II is roughly the same shape as those of II and IV, but the calculated conversions of fraction I fail to fall on a smooth curve. The reason could be the large variance in the particle sizes of this fraction, as it includes all particles over 105 µm in diameter.

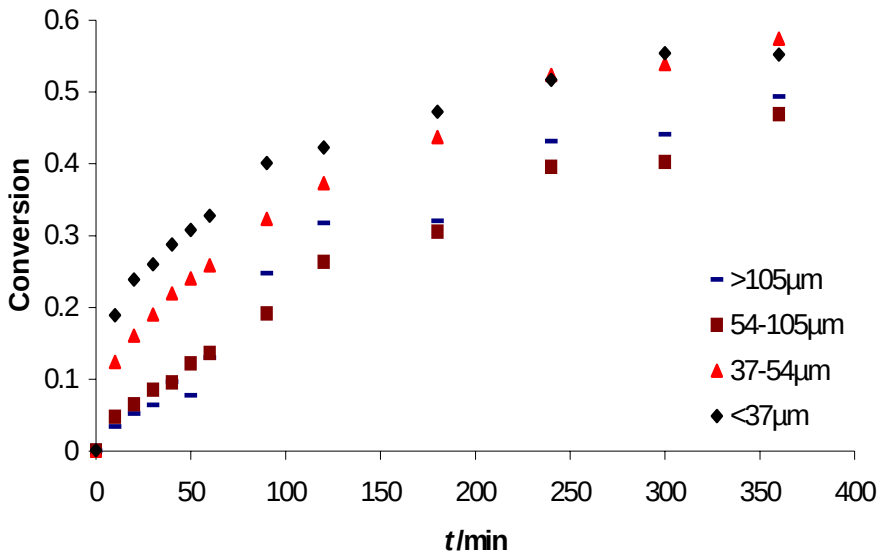

Figure 29. The effect of particle size on conversion. Experiments conducted with 75 mM of Fe in the solution at 80 ℃.

9.4 The effect of iron concentration in the solution

To study the effect of ferric ion concentration in the solution, measurements were carried out in three different initial ferric-ion concentrations: 33, 52 and 75 mmol/l. The conversions calculated from the potentiometric analysis results are expressed as a function of time in figure 30. The measurements were conducted at 60°C and the concentrate size fraction II was used. The results of a potentiometric analysis are expressed, since the AAS analysis results include numerous points, which are clearly out of trend. All of the results are shown in appendix 3.

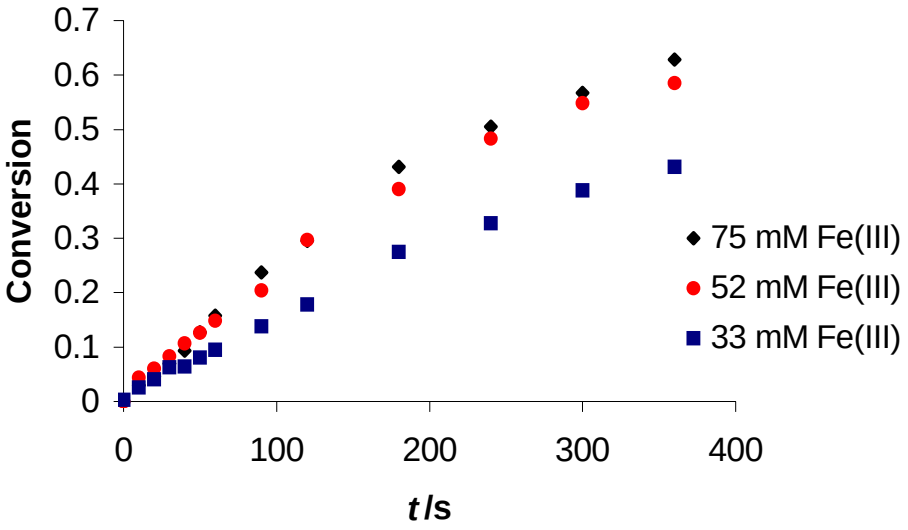

Figure 30. The effect of initial ferric ion concentration on the conversion as a function of time. Experiments conducted with concentrate fraction II at 80 ℃.

As can been seen in the figure, the conversion is greatly enhanced as iron (III) concentration in the solution is increased from 33 mM to 52 mM and thus the overstoichiometry factor from 1.1 to 1.75. When the concentration is further increased to 75mM (factor 2.2), no significant increase in conversion is noted. The same effect could be seen for the measurements in other temperatures, as can be seen in appendix 4. Somewhere between 33 mM and 52mM is to be found a concentration of Fe-(III), up to which the increasing of iron concentration affects the conversion and above which it no longer does so.

9.5 The effect of zinc concentration in the solution

The effect of 100g/l of dissolved zinc in the solution was studied in measurements M17-M20. The measurements were conducted with size fraction II of the concentrate, with 75 mM of ferric ions in the solution at temperatures 60, 70, 80 and 90°C, which are the same parameters as for measurements M9, M6, M10 and M11 respectively. The volume of sulphuric acid for M17-M20 was 1.2 l instead of 1.5 l as in the corresponding measurements, due to the sizeable zinc sulphide addition.

For these experiments, the conversion versus time curves could only be calculated from the measured potentials, as the change in zinc concentration in the solution was too small to be analytically determined. These curves, as well as the curves for corresponding measurements without the zinc addition, are shown in figures 31-34. The residue analysis results are presented in table 5. As can be seen, the combined mass fraction of zinc and sulphur is above 1 in all measurements. As the results are clearly not accurate, they are omitted from further discussion.

Table 5. Results of the residue analysis.

Measurement	**none**	**M17**	**M18**	**M19**	**M20**
Zn m-%	0.497	0.493	0.408	0.374	0.219
S m-%	0.407	0.533	0.652	0.636	0.682

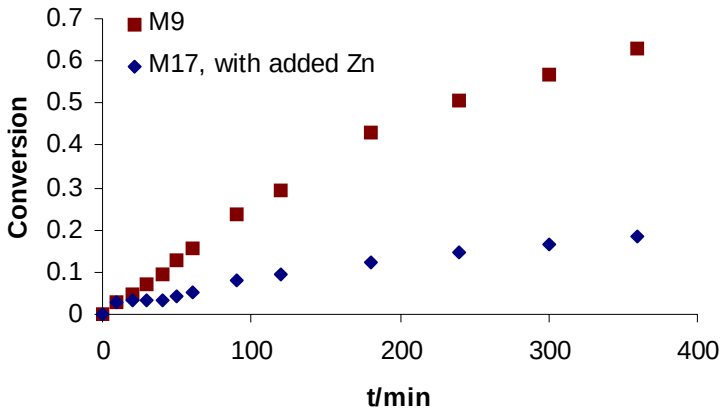

Figure 31. Conversions with and without 100 g/l Zn in the solution. Concentrate fraction II, Fe^{3+} concentration 75 mM, temperature 60 ℃.

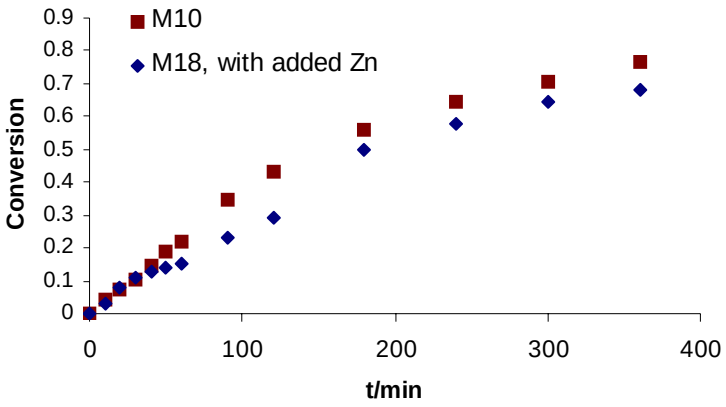

Figure 32. Conversions with and without 100 g/l Zn in the solution. Concentrate fraction 57-103µm, Fe^{3+} concentration 75 mM, temperature 70 ℃.

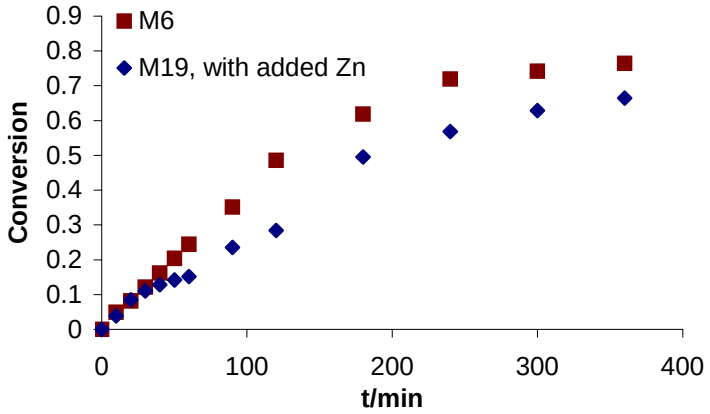

Figure 33. Conversions with and without 100 g/l Zn in the solution. Concentrate fraction 57-103µm, Fe^{3+} concentration 75 mM, temperature 80 ℃.

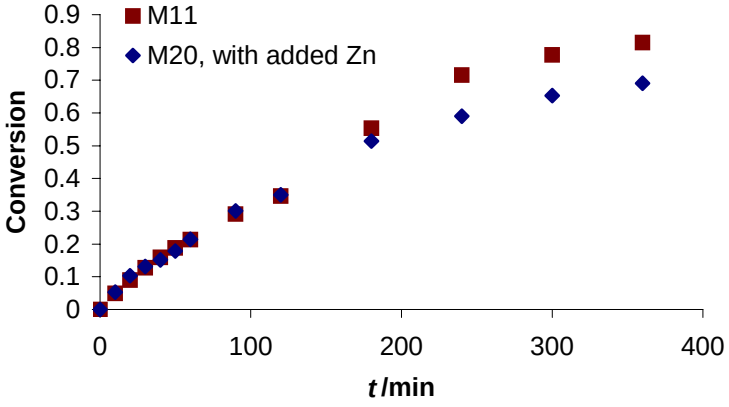

Figure 34. Conversions with and without 100 g/l Zn in the solution. Concentrate fraction 57-103µm, Fe^{3+} concentration 75 mM, temperature 90 ℃.

As can be seen in figure 31, at 60°C the rate of dissolution in dramatically decreased by the presence of 100 g/l dissolved zinc in the solution. The final conversion decreases by 67 % and the two conversion curves are clearly separated after only 20 minutes. At temperatures 70°C and 80°C, the separation takes place after 40 minutes and the final conversion is decreased by 15 %. At 90°C, the decrease in final conversion is of the same magnitude as at 70°C and 80°C, however the separation of curves is not noted until after 180 min. Once again the results for measurements at 60°C differ greatly from the results at higher temperatures, which seems to indicate a change in the prevailing reaction mechanism.

9.6 The effect of stirring

To study the effect of stirring, measurement M6 was repeated with stirring set at 500 rpm. This rate of stirring was just enough to keep the solids dispersed in the solution. The conversions calculated from the analysis results are expressed in figure 35.

From the figure it can be seen that, surprisingly, the conversions reached were greater in the experiment with less intensive stirring. However, the differences were not great, and the final conversions after 6 hours were equal. The value at 300 minutes with 1000 rpm mixing is clearly out of trend and if this point is ignored, the effect of the stirring rate is negligible.

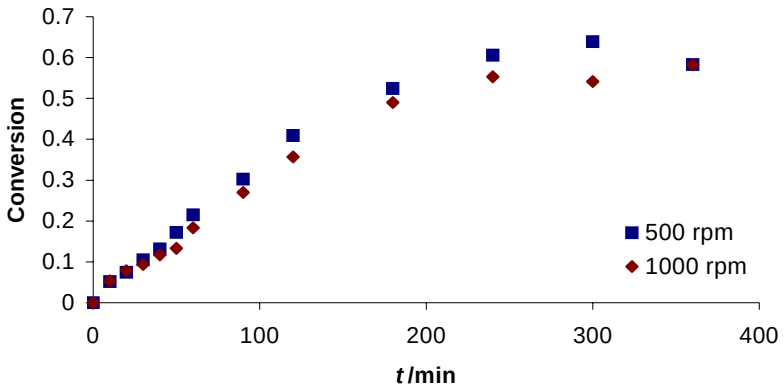

Figure 35. The effect of stirring on conversion. Measurements were carried out with fraction II of the concentrate, 75 mM Fe in the solution, at 80 ℃.

No explanation was found to why greater conversions were reached with lesser stirring; however, two separate reasons could explain why the conversions did not grow with increased stirring. Firstly, the abundance of ferric ions in the solution could prevent the diffusion in the solution from becoming the rate-determining step at any point during the measurement. This would eliminate the effect of stirring on the rate of dissolution. Secondly, both rates of stirring may be inadequate for essentially decreasing the thickness of the diffusion layer surrounding any particle. An experiment with a considerably higher rate of stirring should be carried out, to see whether the rate of stirring does affect the rate of dissolution.

9.7 Dissolution kinetics

In order to determine the reaction mechanisms, equations (1) and (3) were fitted to the data. The rate of reaction is determined by the surface reaction in the case of equation (1) and by diffusion through the product layer in equation (3). In figures 36, 37, 38 and 39 are these equations fitted to the data of measurements M9, M10, M6 and M11, where the initial ferric ion concentration is 75mM, the concentrate fraction used is 57-103µm and the temperatures are 60, 70, 80 and 90°C respectively. For the rest of the measurements, the fittings can be seen in appendix 4. In most cases the dissolution initially proceeds by mechanism (1) and subsequently continues by mechanism (2). In some cases, however, the data fails to obey either equation, or both equations give an equally good fit over the whole timescale.

From figure 36 on page 61 it can be seen that at 60°C the surface reaction is the rate-determining step for the first 90 minutes of dissolution, while diffusion becomes dominant after 2 hours. In between, from 90 minutes to 120 minutes, both equations explain the data equally well as the mechanism changes from surface reaction control to diffusion control.

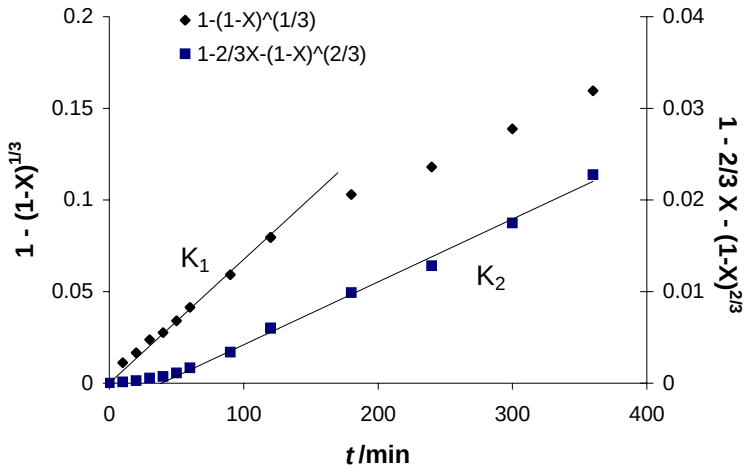

Figure 36. The fitting of equations (1) and (3) to the data of M9. Ferric ion concentration 75mM, concentrate fraction II, temperature 60℃. K_1 = 0.0007 min^{-1} and K_2 = 0.00007 min^{-1}.

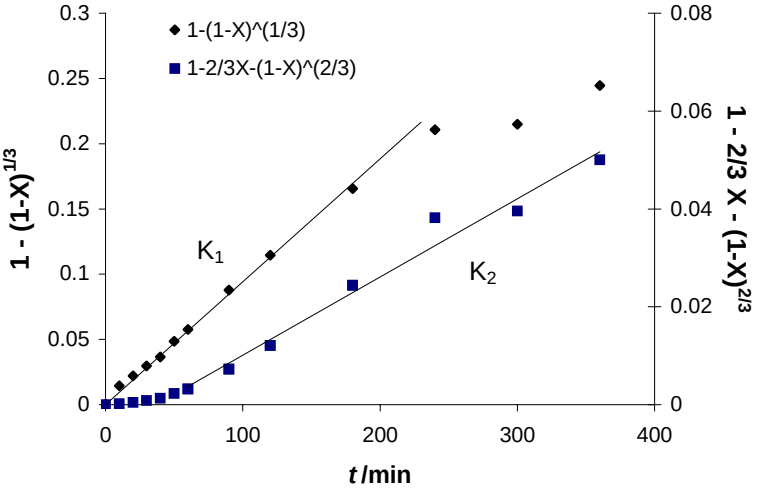

Figure 37. The fitting of equations (1) and (3) to the data of M10. Ferric ion concentration 75mM, concentrate fraction II, temperature 70℃. K_1 = 0.0009 min^{-1} and K_2 = 0.0002 min^{-1}.

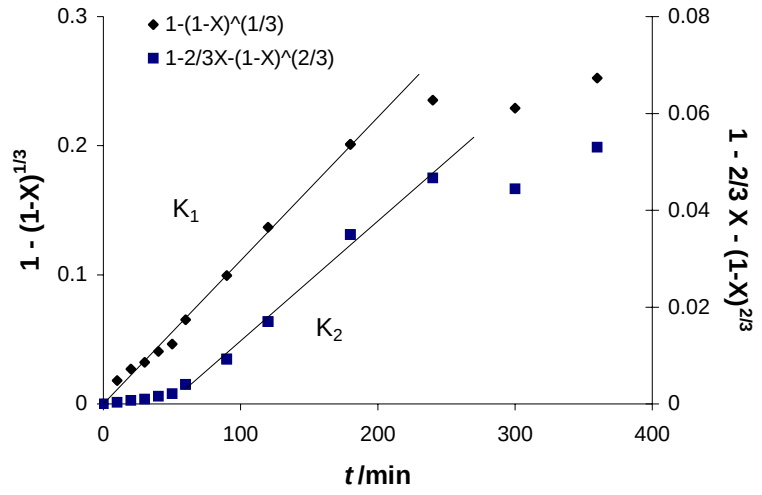

Figure 38. The fitting of equations (1) and (3) to the data of M6. Ferric ion concentration 75mM, concentrate fraction II, temperature 80℃. K_1 = 0.0011 min^{-1} and K_2 = 0.0002 min^{-1}.

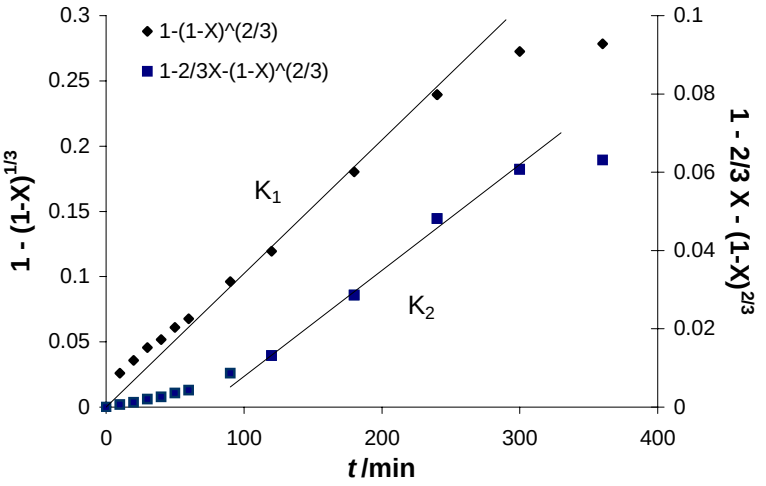

Figure 39. The fitting of equations (1) and (3) to the data of M11. Ferric ion concentration 75mM, concentrate fraction II, temperature 90℃. K_1 = 0.001 min^{-1} and K_2 = 0.0003 min^{-1}.

From figures 37, 38 and 39 it can be seen that as the temperature is increased, the equation for surface reaction control (1) is obeyed for a longer period of time. The equation for diffusion control (2) becomes linear at a later time at higher temperatures and an increasing trend in the apparent rate constants K_1 and K_2 can be observed.

9.8 The repeatability of measurements

Although none of the experiments were repeated as such, the repeatability of these measurements can be studied, since there was only a slight change in the conversions between ferric ion concentrations 52 mM and 75 mM. In figure 40 the conversions are calculated from the potentials for these concentrations of ferric ions at temperatures 60 and 80°C.

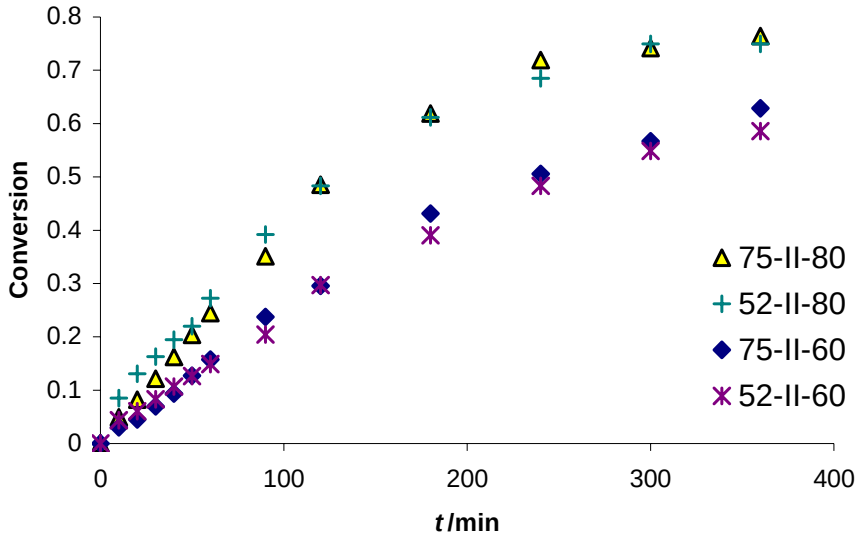

Figure 40. The repeatability of measurements, correlation of measurements M6 and M9 with M3 and M1.

As can be seen, the curves are close to identical in both temperatures. This would indicate that this method is repeatable. Once the discrepancy between the AAS analysis and the potentiometric analysis is resolved, the proposed method can be used for convenient real-time analysis of the reaction solution.

10 SUMMARY

The subject of this study was the atmospheric, oxidative leaching of sphalerite concentrates in sulphuric acid with ferric sulphate. One of the objectives was to develop an *in-situ* method for monitoring this dissolution process, based on measuring the potential set by the ferric/ferrous ion ratio in the solution. Another purpose of the measurements was to study the effect of different variables on the rate of dissolution.

A series of 6 hour dissolution experiments were carried out in oxygen-free sulphuric acid solutions containing ferric sulphide. Four size fractions of one Outokumpu Pyhäsalmi concentrate were used and experiments were conducted at temperatures 60°C, 70°C, 80°C and 90°C. Other variables under study were the rate of stirring and the concentrations of zinc and ferric ions in the solution.

A potentiometric method for the *in-situ* monitoring of the ZnS oxidative dissolution process was introduced and tested. During the dissolution experiments, the potential difference between a platinum electrode and a Ag/AgCl reference electrode was measured, and the conversion of zinc sulphide to dissolved zinc was calculated. The results obtained with this method differ by about 20 % from those obtained from sample AAS analysis. However, the shapes of the conversion versus time curves were similar and the discrepancy could be eliminated with the use of a correction factor.

A propable explanation for the discrepancies is the presence of another oxidation reaction, which uses Fe^{3+} as the oxidant. The proposed reaction is the oxidation of elemental sulphur to the sulphate ion. Due to the inaccuracy of the sulphur analysis performed, this proposition could not be verified or contradicted, and further studies have to be carried out to fully research this possibility. If the dissolution of sulphur is the cause for the differences between the potentiometric and the AAS analysis results, these differences could be used to calculate the extent of the sulphur oxidation reaction.

The results of the dissolution experiments show that increasing the temperature from 60°C to 70°C increases the rate of dissolution considerably. Raising the temperature further to 80°C or 90°C had only a slight effect on the rate of dissolution and the conversions reached. This would suggest a change in the reaction mechanism from kinetically controlled to diffusion controlled. This would also suggest that experiments conducted at some temperature above 70°C would be valid at least within the temperature range 70°C-90°C. Below this range the dissolution mechanism is changed and at above 100°C the boiling of the solvent complicates the experiments and the interpretation of the results.

The results of the experiments, where the effect of particle size on the rate of dissolution was studied, were quite expected; the rate increased with the decease of particle size. Decreasing the rate of stirring from 1000 rpm to 500 rpm had no significant effect on the conversions, which could indicate that both rates were insufficient in decreasing the thickness of the diffusion layer surrounding the particle. A measurement should be conducted with a considerably higher stirring rate, to see if this is the case. An experiment to study the effect of stirring rate should also be carried out in a solution with a lower concentration of ferric ions, to find out if still no change in the dissolution rate is observed.

As the iron content in the solution was raised from 33 mM to 52 mM, a significant increase in the conversion was noted, while a further increase to 75 mM had practically no effect. It can be concluded that the concentration of ferric ions only effects the dissolution up to an overstoichiometry of 1.75. The effect of zinc concentration was studied and at temperatures 70°C, 80°C and 90°C, the effect of 100 g/l of dissolved zinc in the solution was a 15 % decrease in conversions. At 60°C a decrease of 67 % was noted, which once again suggests that experimental results obtained at 60°C should not be generalised to apply at higher temperatures.

Two rate equations were fitted to the experimental data, and the results suggest that the rate of dissolution is first controlled by the reaction taking place at the mineral surface, while diffusion through a product layer becomes the rate-determining step at latter stages of the dissolution.

11 REFERENCES

1. Anon., Products: Zinc, http://www.outokumpu.com/metallurgy/zinc.htm, 19.2.2002.
2. Takala, H., Leaching of zinc concentrates at Outokumpu Kokkola plant, *Erzmetall* **52** (1) (1999) 37-42.
3. Rytioja, A., *Sinkkirikasteen suoraliuotus, rikasteiden liukenevuuden testausmenetelmän kehitys*, Diplomityö, Oulun Yliopisto, Prosessitekniikan osasto, Oulu 1997, 79 p.
4. Haung, H.H., Bernal, J.E., Kinetic study on direct leaching of sphalerite in sulfuric acid solution using ferrous sulfate as the catalyst, *Proc. - Electrochem. Soc.* **84-10** (1984) (*Proc. Int. Symp. Electrochem. Miner. Met. Process., 1984)* 469-485.
5. Srinivasan, G.N., Venkatakrishna Iyer, S., Cyclic voltammetric studies on sphalerite electrodes, *Bulletin of Electrochemistry* **16** (1) (2000) 5-9.
6. Kantanen, H., *Sinkkirikasteiden liukenemisnopeuksien vertailu*, Raportti 96111-ORC-T, Outokumpu Research Oy, Pori 1996, 13 p.
7. Veltman, M., Bolton, G.L., Direct pressure leaching of zinc blende with simultaneous production of elemental sulphur. A state-of-the-art review, *Erzmetall* 33 (2) (1980) 76-83.
8. Jan, R.J., Hepworth, M.T., Fox, V.G., A kinetic study on the pressure leaching of sphalerite, *Metallurgical Transactions B* **7B** (1976) 353-361.
9. Corriou, J.P., Gely, R., Viers, P., Thermodynamic and kinetic study of the pressure leaching of zinc sulfide in aqueous sulfuric acid, *Hydrometallurgy* **21** (1988) 85-102.
10. Dreisinger, D.B., Peters, E., The oxidation of ferrous sulphate by molecular oxygen under zinc pressure-leach conditions, *Hydrometallurgy* **22** (1989) 101-119.
11. Dutrizac, J.E., Meacdonald, R.J.C., The dissolution of sphalerite in ferric chloride solutions, *Metallurgical Transactions* **9 B** (1978) 543-551.
12. Zuo-Mei Jin, Warren, G.W., Henein, H., Reaction kinetics of the ferric chloride leaching of sphalerite – an experimental study, *Metallurgical Transactions B* **15B** (1984) 5-12.

13. Bobeck, G., Su, H., The kinetics of dissolution of sphalerite in ferric chloride solution, *Metallurgical Transactions* **16 B** (1985) 413-424.
14. Suni, J., Henein, H., Warren, G.W., Reddy, D., Modelling the leaching kinetics of sphalerite concentrate size distribution in ferric chloride solution, *Hydrometallurgy* **22** (1989) 25-38.
15. Suzuki, I., Microbial leaching of metals from sulfide minerals, *Biotechnology Advances* **19** (2001) 199-132.
16. Selvi, S.C., Modak, J.M., Natarajan, K.A., Technical note: Electrobioleaching of sphalerite flotation concentrate, *Minerals Engineering* **11** (8) (1998) 783-788.
17. Fowler, T.A., Crundwell, F.K., Leaching of zinc sulfide by thiobacillus ferrooxidans: bacterial oxidation of the sulfur product layer increases the rate of zinc sulfide dissolution at high concentrations of ferrous ions, *Applied and Environmental Microbiology* **65** (12) (1999) 5285-5292.
18. Crundwell, F.K., Kinetics and mechanism of the oxidative dissolution of zinc sulphide consentrate in ferric sulphate solutions, *Hydrometallurgy* **19** (1987) 227-242.
19. Crundwell, F.K., Refractory behaviour of two sphalerite concentrates to dissolution in ferric sulphate solutions, *Hydrometallyrgy* **19** (1987) 253-258.
20. Lochmann, J., Pedlik, M., Kinetic anomalities of dissolution of sphalerite in ferric sulfate solution, *Hydrometallurgy* **37** (1995) 89-96.
21. Taskinen, P., *Suoraliuotusreaktorin mallinnuksen tutkijaseminaari*, Report 01126-ORC-M, Outokumpu Research Oy, Pori 2001, 4p.
22. Ahlberg, E., Asbjörnsson, J., Carbon paste electrodes in mineral processing: an electrochemical study of sphalerite, *Hydrometallurgy* **36** (1994) 19-37.
23. Palencia Perez, I., Dutrizec, J.E., The effect of the iron content of sphalerite on its rate of dissolution in ferric sulphate and ferric chloride media, *Hydrometallurgy* **26** (1991) 211-232.
24. Lapidus, G., De Lourdes Mosqueira, M., The effect of product solubility on the leaching kinetics of non-porous minerals, *Hydrometallurgy* **20** (1988) 49-64.

25. Munoz, Miller, Wadsworth, Reaction mechanism for the acid ferric sulfate leaching of chalcopyrite, *Met. Trans.* **10 B** (1979) 149-158.
26. Choi, W-K., Torma A.E., Electrochemical charecterization of a semiconductor ZnS concentrate during oxidative leaching, in: Lakshmann, V.I. (Ed.), *Advanced Materials - Application of Mineral and Metallurgial Processing Principles*. Society for Mining, Metallurgy and Exploration Inc., Littleton, Colorado 1990, p. 95-107.
27. Mortimer, R.G., *Physical Chemistry*, The Benjamin/Cummings Publishing Company, Inc., New York 1993, 977-984.
28. Halavaara, P., *Sinkkirikasteen liukenemisnopeuteen vaikuttavat tekijät*, Diplomityö, Lappeenrannan Teknillinen Korkeakoulu, Kemiantekniikan Osasto, Lappeenranta 1996, 70 p.
29. Kammel, R., Pawlek, F., Simon, M., Xi-Ming, L., Oxidizing leaching of sphalerite under atmospheric pressure, *Metall* 41 (2) (1987) 158-161.
30. Verbaan, B., Crundwell, F.K., An electrochemical model for the leaching of a sphalerite concentrate, *Hydrometallurgy* **16** (1986) 345-359.
31. Palencis, I., Carranza, F., Garcia, M.J., Leaching of a copper – zinc bulk sulphide concentrate using an aqueous ferric sulphate dilute solution in a semicontinopus system. Kinetics of dissolution of zinc, *Hydrometallurgy* **23** (1990) 191-202.
32. Gely, R., Corriou, J-P., Viers, P., Etude thermodynamique et cinetique de la lixiviation du sulfure de zinc en solution aqueuse d'acide sulfurique, *Bull. Soc. Chim. Fr.* **3** (1987) 405-412.
33. Balaz, P., Ebert, I., Oxidative leaching of mechanically activated sphalerite, *Hydrometallurgy* **27** (1991) 141-150.
34. Nowak, P., Sulfide sulfur transformations in the processes of the oxidation of metal sulfide's surface, *Technol. Chem. Przelomie Wiekow* (2000) 295-298.
35. Pesonen, P., *Sulfidimineraalien liukenemisen sähkökemiallinen diagnosointimetodiikka*, Lisensiaattitutkimus, Teknillinen Korkeakoulu, Materiaali- ja Kalliotekniikan osasto, Espoo 2000, 87 p.
36. Mortimer, R.G., *Physical Chemistry*, The Benjamin/Cummings Publishing Company, Inc., Redwood City 1993, 295-305.

37. Knuutila, K., Forsen, O., Mineraalisulfidien liuotuksen kinetiikkaa hapettavissa olosuhteissa, in: Järvinen, O. (Ed.), *Metallurgisten Prosessien Kinetiikasta*, Report TKK-V-C63, Otaniemi 1986, p. 27-66.

38. Buckley, A.N., Wouterlood, H.J., Woods, R., The surface composition of natural sphalerites under oxidative leaching conditions, *Hydrometallurgy* **22** (1989) 39-56.

39. Bockris, J. O'M., Khan, S.U.M., *Surface Electrochemistry - A molecular level approach*, Plenum Press, New York 1993, p.750-753

40. Madhuchhanda, M., Devi, N.B., Rao, K.S., Rath, P.C., Paramguru, R.K., Galvanic interaction between sulfide minerals and pyrolusite, *J. Solid State Electrochem.*, **4** (2000) 189-198.

41. Jones, D.A., Paul, A.J.P., Galvanic interactions between alloys and minerals in sulfuric acid, *Corrosion* **50** (7) (1994) 516-521.

42. Crundwell, F.K., The influence of electronic structure of solids on the anodic dissolution and leaching of semiconducting sulphide minerals, *Hydrometallurgy* **21** (1988) 155-190.

43. Zhang, S., Choi, W.K., Torma, A.E., Kinetics of leaching of a zinc sulfide flotation concentrate with HCl/$FeCl_3$ solutions, *Metall* **42** (9) (1988) 881-884.

44. Koch, D.F.A., Electrochemistry of sulfide minerals, in: Bockris, J. O'M., Conway, B. E., *Modern Aspects of Electrochemistry* **10** (1975) 211-237.

45. Bockris, J.O.M., Reddy, A.K.M., *Modern electrochemistry vol. 2*, Plenum Press, New York, 1970, 803-824.

46. West, A. R., *Solid state chemistry and its applications*, John Wiley & Sons, Chichester 1987, 319-326 and 497-504.

47. Sundholm, G., *Sähkökemia*. Otakustantamo 502, Espoo 1987, s. 100-105.

48. Mikhlin, Yu., Tomashevich, Ye., Asanov, Okotrub, A., Effect of surface non-stoichiometry on the dissolution of metal sulfides in *Electrochemistry in mineral and metal processing V*. Proceedings Vol. 2000-14, The Electrochemical Society, USA 2000, 283-292.

49. Knuutila, K., Aromaa, J., Forsen, O., *Mineraalisulfidien puolijohdeominaisuuksien vaikutus sähkökemialliseen liukenemiseen*. Report TKK-V-C44, Otaniemi 1985, 48 p.

50. Peters, E., Direct leaching of sulfides: chemistry and applications, *Metallurgical Transactions B* **7B** (1976) 505-517.

51. Owusu, G., Dreisinger, D.B., Peters, E., Effect of surfactants on zinc and iron dissolution rates duriong oxidative leaching of sphalerite, *Hydrometallurgy* **38** (1995) 315-324.

52. Toniazzo, V., Mustin, C., Portal, J.M., Humbert, B., Benoit, R., Erre, R., Elemental sulfur at the pyrite surfaces: speciation and quantification, *Applied Surface Science* **143** (1999) 229-237.

53. Bard, A.J., Faulkner, L.R., *Electrochemical Methods : Fundamentals and Applications*, John Wiley & Sons, Inc., USA 2001, 669-677.

Appendix 1. The measurement apparatus.

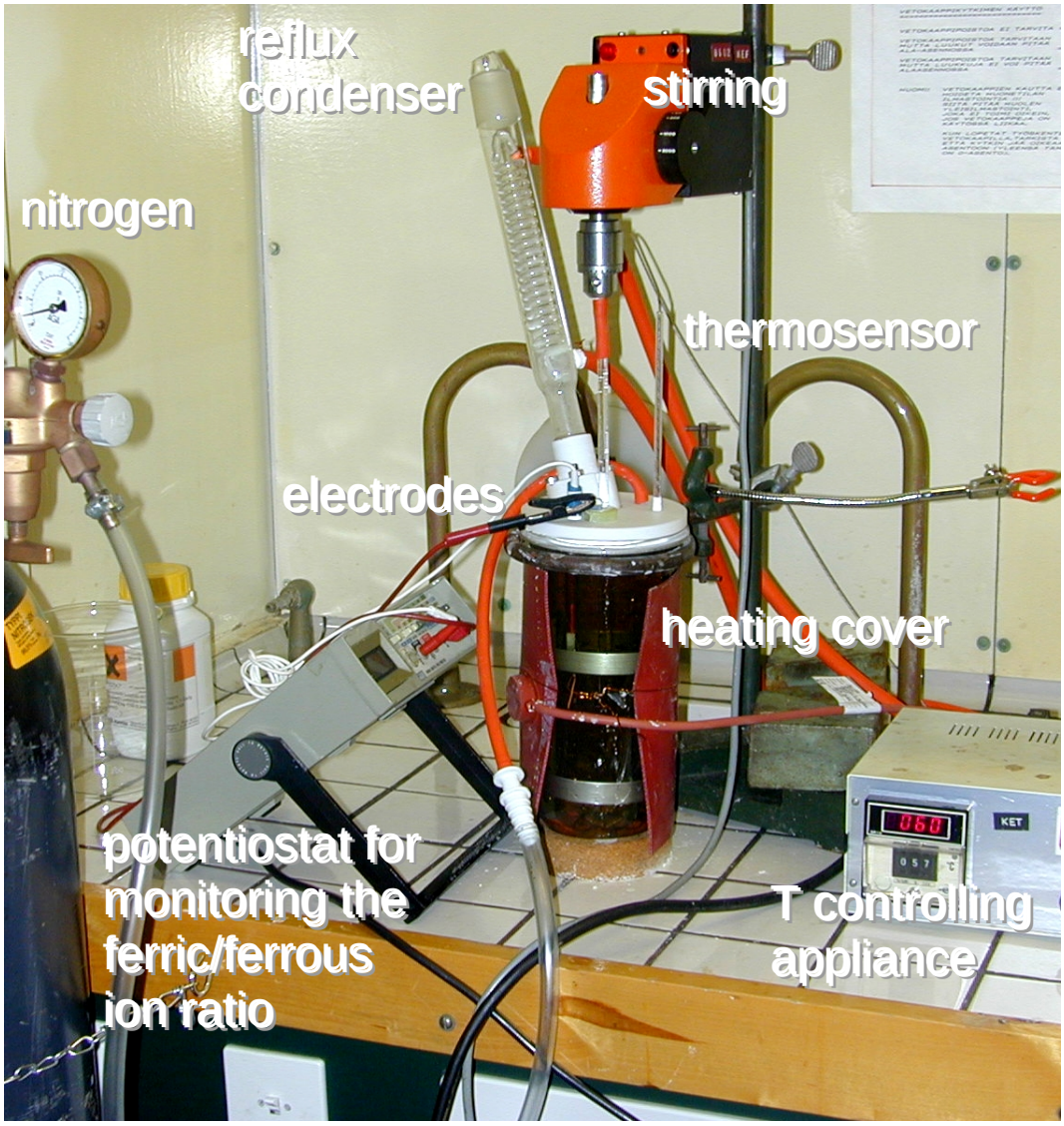

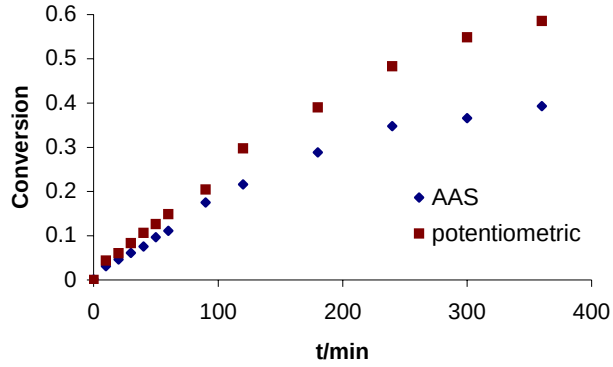

Measurement		M1
Fe (III)	mM	52
Fraction	µm	54-105
Temperature	°C	60
V	dm^3	1.2

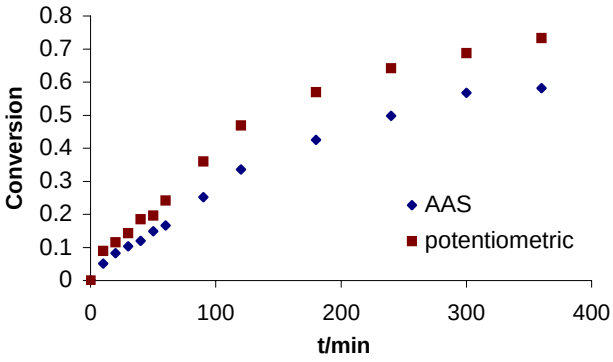

Measurement		M2
Fe (III)	mM	52
Fraction	µm	54-105
Temperature	°C	70
V	dm^3	1.2

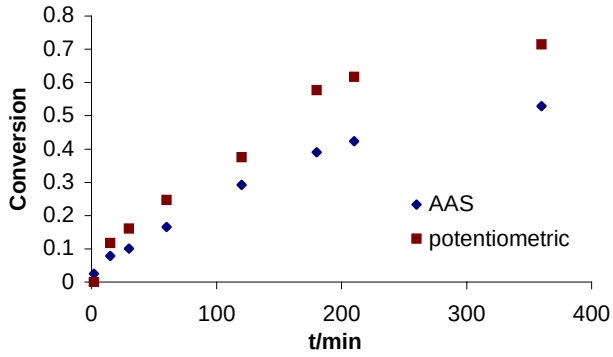

Measurement		M3
Fe (III)	mM	52
Fraction	µm	54-105
Temperature	°C	80
V	dm^3	1.2

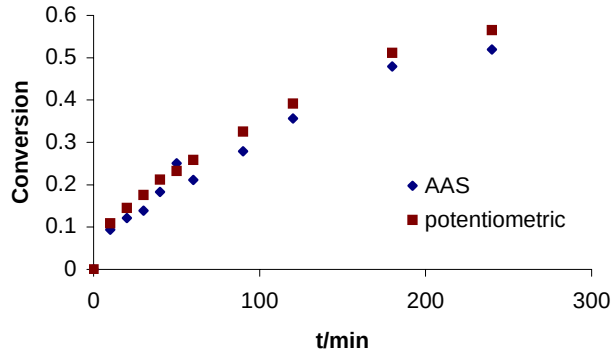

Measurement		M4
Fe (III)	mM	52
Fraction	µm	54-105
Temperature	°C	90
V	dm^3	1.2

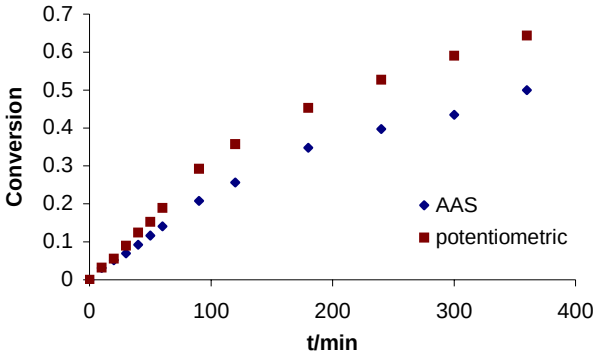

Measurement		M5
Fe (III)	mM	75
Fraction	µm	>105
Temperature	°C	80
V	dm^3	1.5

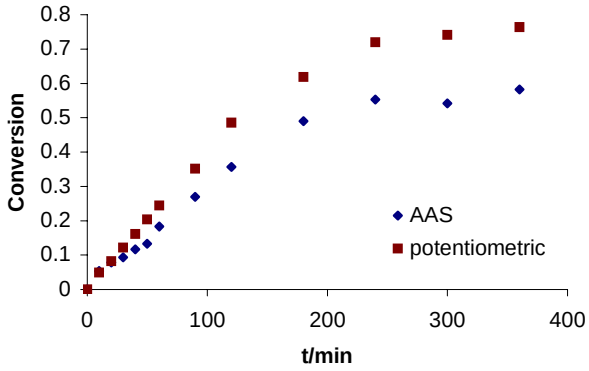

Measurement		M6
Fe (III)	mM	75
Fraction	µm	54-105
Temperature	°C	80
V	dm^3	1.5

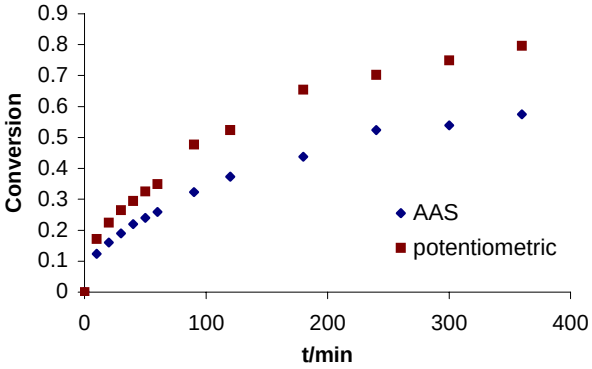

Measurement		M7
Fe (III)	mM	75
Fraction	µm	37-54
Temperature	°C	80
V	dm^3	1.5

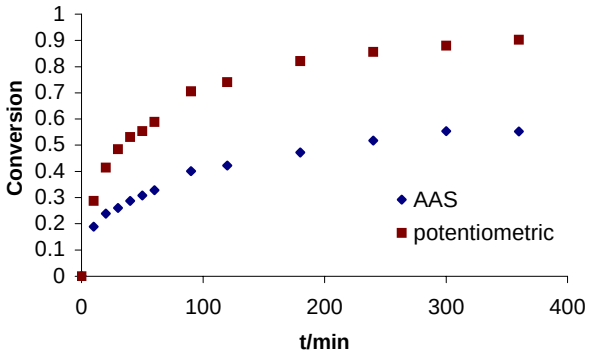

Measurement		M8
Fe (III)	mM	75
Fraction	µm	<37
Temperature	°C	80
V	dm^3	1.5

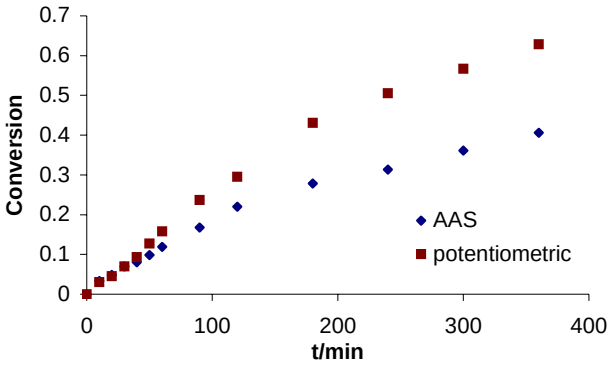

Measurement		M9
Fe (III)	mM	75
Fraction	µm	54-105
Temperature	°C	60
V	dm^3	1.5

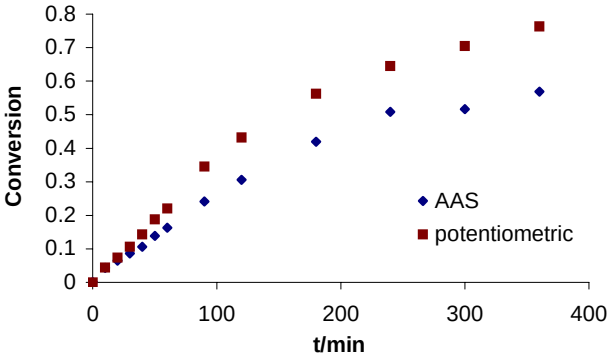

Measurement		M10
Fe (III)	mM	75
Fraction	µm	54-105
Temperature	°C	70
V	dm^3	1.5

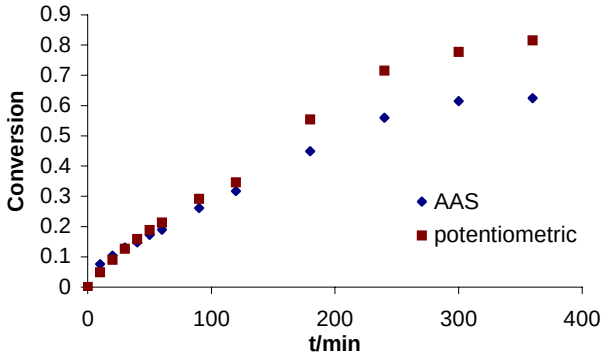

Measurement		M11
Fe (III)	mM	75
Fraction	µm	54-105
Temperature	°C	90
V	dm^3	1.5

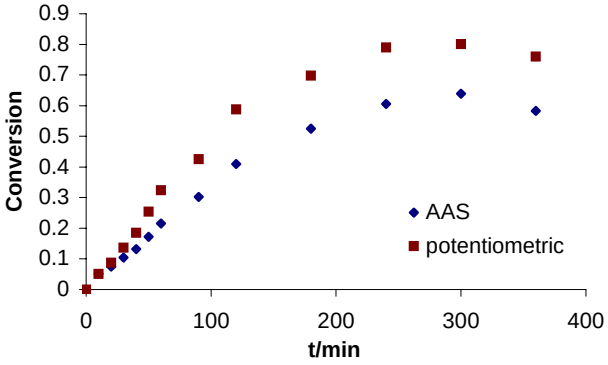

Measurement		M16
Fe (III)	mM	75
Fraction	µm	54-105
Temperature	°C	90
V	dm^3	1.5

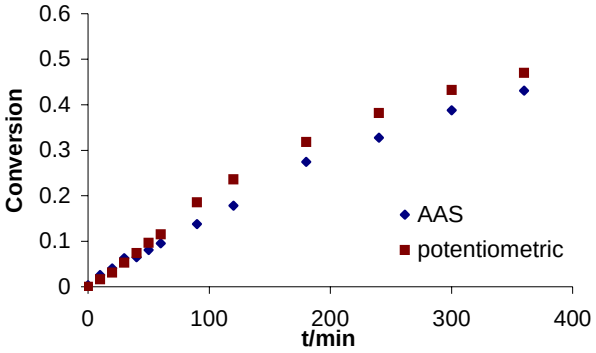

Measurement		M12
Fe (III)	mM	33
Fraction	µm	54-105
Temperature	℃	60
V	dm^3	1.2

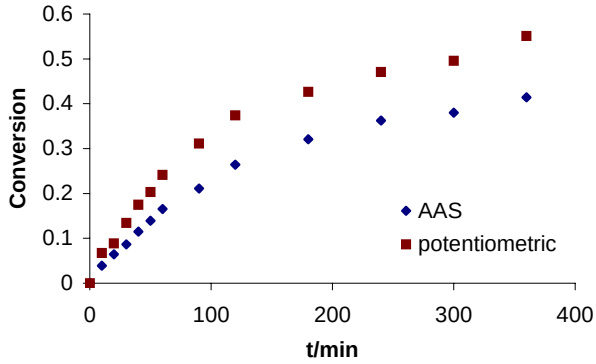

Measurement		M13
Fe (III)	mM	33
Fraction	µm	54-105
Temperature	℃	70
V	dm^3	1.2

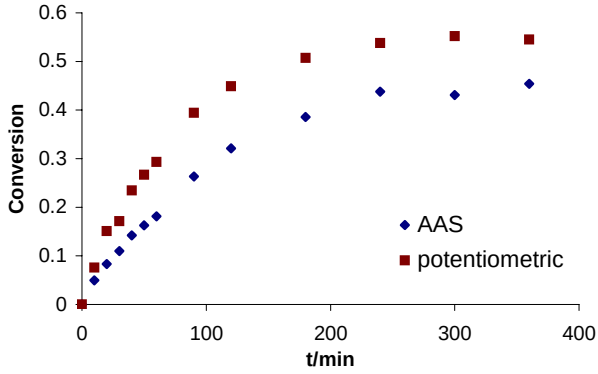

Measurement		M14
Fe (III)	mM	33
Fraction	µm	54-105
Temperature	℃	80
V	dm^3	1.2

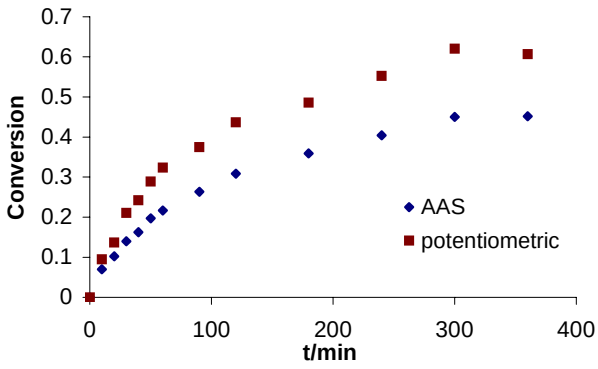

Measurement		M15
Fe (III)	mM	33
Fraction	µm	54-105
Temperature	℃	90
V	dm^3	1.2

Appendix 3. The conversions calculated from the potentiometric and the AAS analysis results at iron concentrations 33 mM, 52 mM and 75 mM.

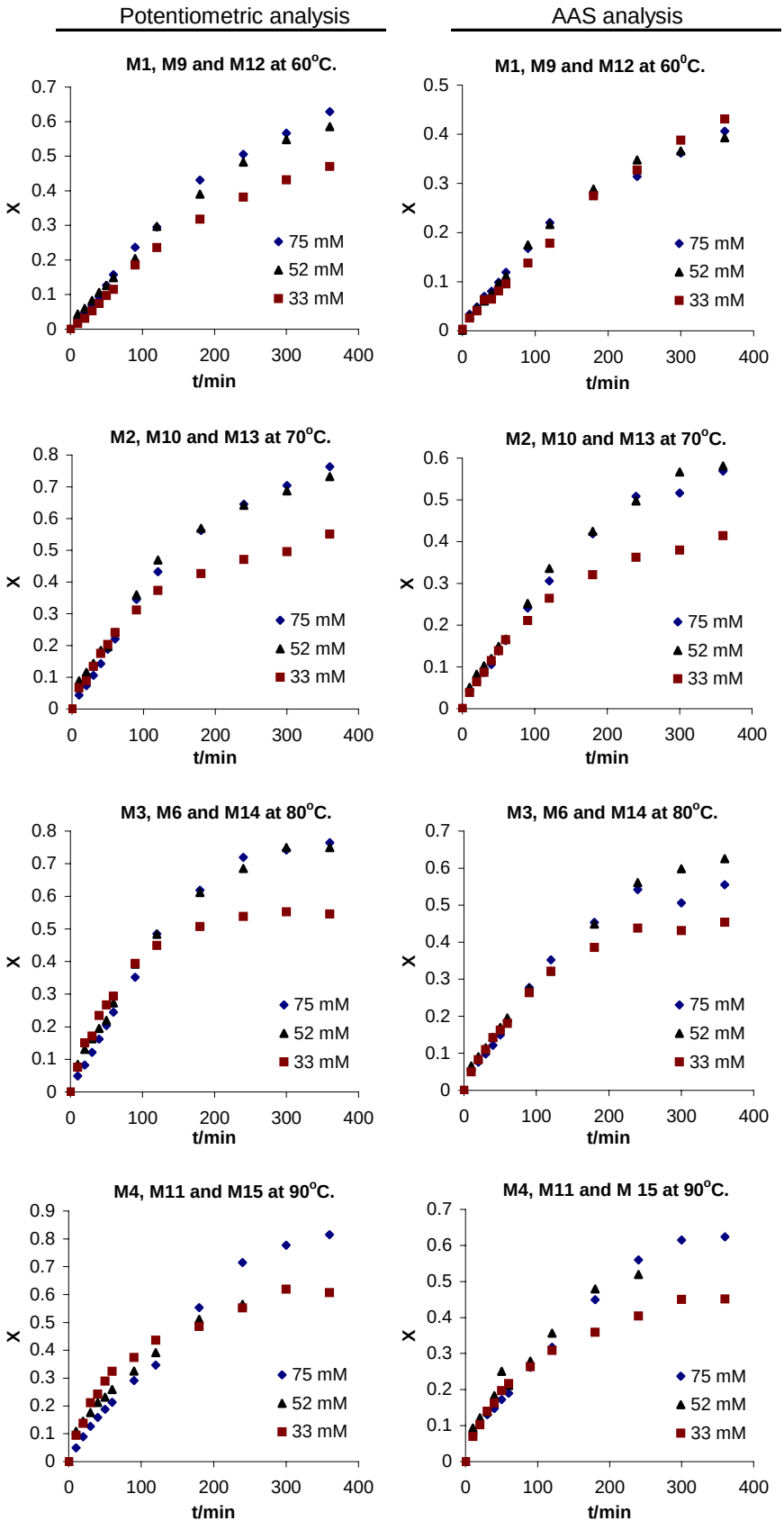

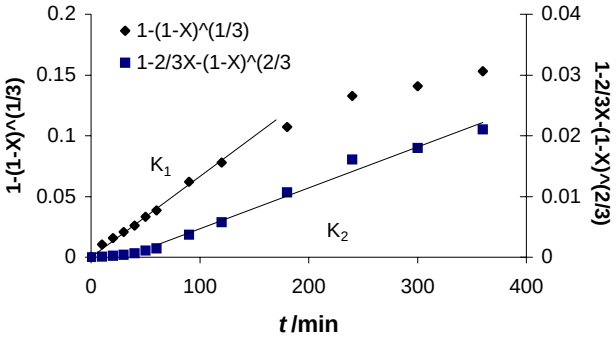

Measurement		M1
Fe (III)	mM	52
Fraction	µm	54-105
Temperature	°C	60
V	dm^3	1.2
K_1	1/min	0.0007
R^2_1		0.9932
K_2	1/min	0.00007
R^2_2		0.98274

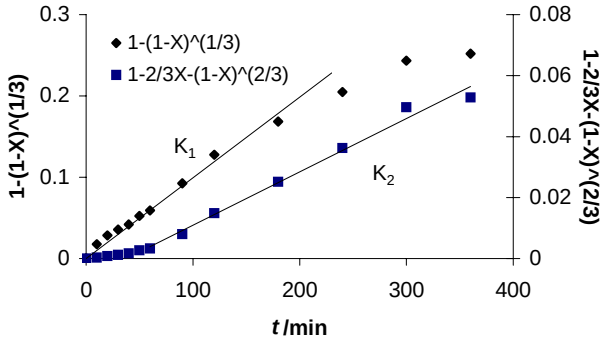

Measurement		M2
Fe (III)	mM	52
Fraction	µm	54-105
Temperature	°C	70
V	dm^3	1.2
K_1	1/min	0.001
R^2_1		0.9854
K_2	1/min	0.0002
R^2_2		0.9872

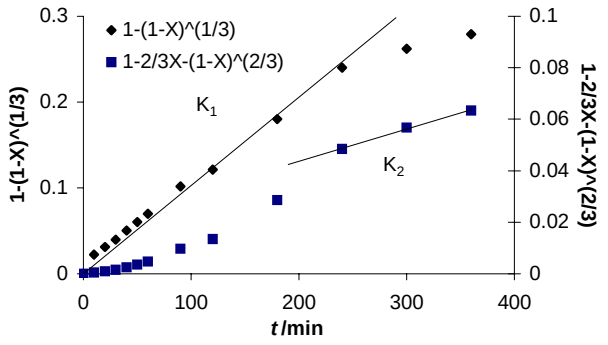

Measurement		M3
Fe (III)	mM	52
Fraction	µm	54-105
Temperature	°C	80
V	dm^3	1.2
K_1	1/min	0.001
R^2_1		0.986
K_2	1/min	0.0001
R^2_2		0.9959

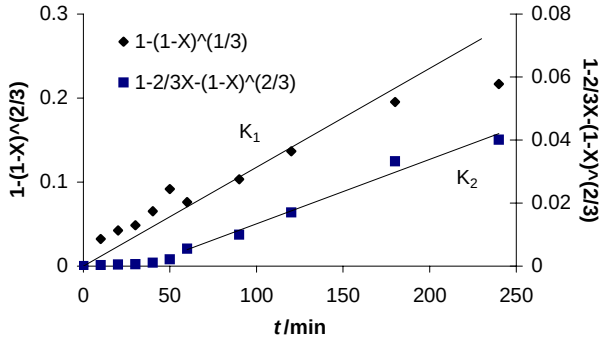

Measurement		M4
Fe (III)	mM	52
Fraction	µm	54-105
Temperature	°C	90
V	dm^3	1.2
K_1	1/min	0.0012
R^2_1		0.9064
K_2	1/min	0.0002
R^2_2		0.98

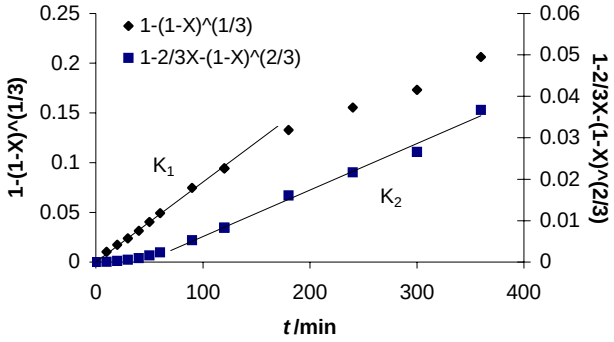

Measurement		M5
Fe (III)	mM	75
Fraction	µm	>105
Temperature	°C	80
V	dm^3	1.5
K_1	1/min	0.0008
R^2_1		0.9974
K_2	1/min	0.0001
R^2_2		0.9846

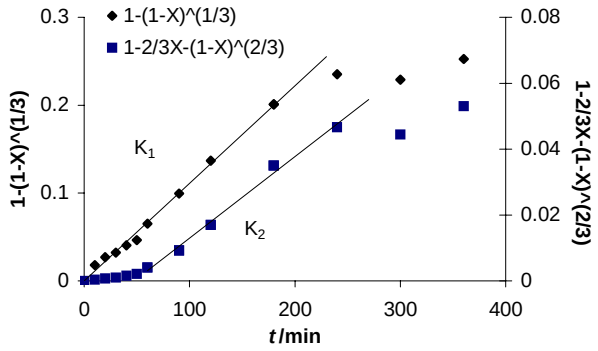

Measurement		M6
Fe (III)	mM	75
Fraction	µm	54-105
Temperature	°C	80
V	dm^3	1.5
K_1	1/min	0.0011
R^2_1		0.9947
K_2	1/min	0.0002
R^2_2		0.9929

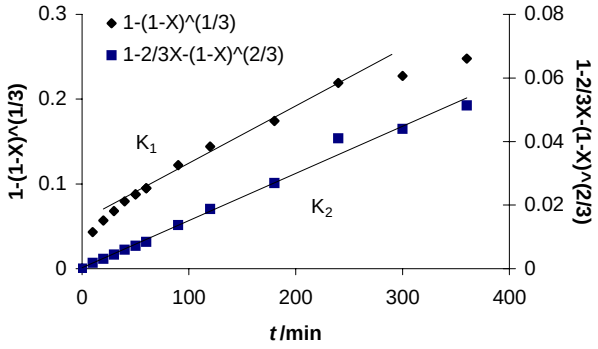

Measurement		M7
Fe (III)	mM	75
Fraction	µm	37-54
Temperature	°C	80
V	dm^3	1.5
K_1	1/min	0.0007
R^2_1		0.9927
K_2	1/min	0.0001
R^2_2		0.9909

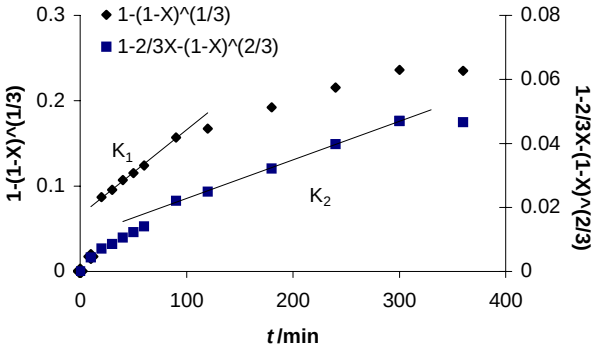

Measurement		M8
Fe (III)	mM	75
Fraction	µm	<37
Temperature	°C	80
V	dm^3	1.5
K_1	1/min	0.001
R^2_1		0.9977
K_2	1/min	0.0001
R^2_2		0.9991

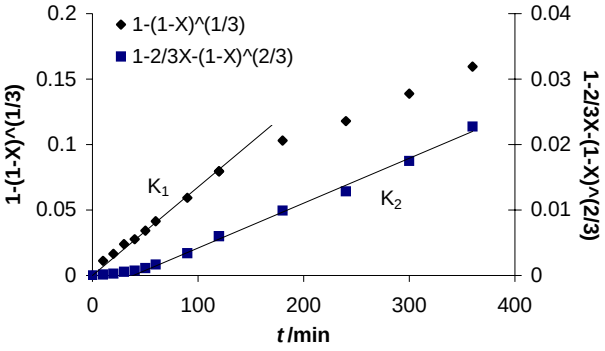

Measurement		M9
Fe (III)	mM	75
Fraction	µm	54-105
Temperature	°C	60
V	dm^3	1.5
K_1	1/min	0.0007
R^2_1		0.9902
K_2	1/min	0.00007
R^2_2		0.9889

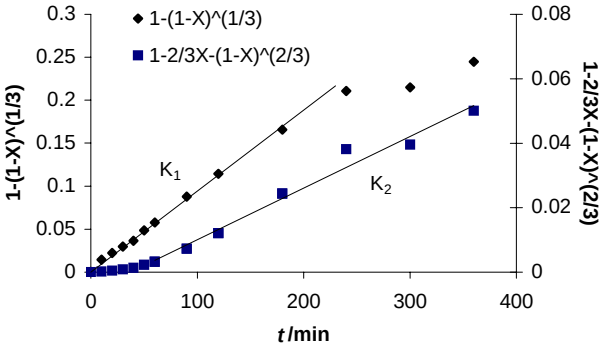

Measurement		M10
Fe (III)	mM	75
Fraction	µm	54-105
Temperature	°C	70
V	dm^3	1.5
K_1	1/min	0.0009
R^2_1		0.9984
K_2	1/min	0.0002
R^2_2		0.9762

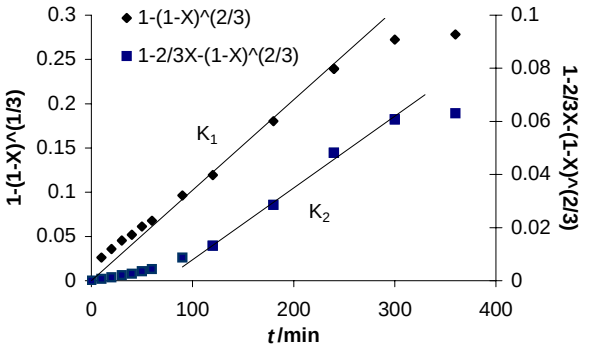

Measurement		M11
Fe (III)	mM	75
Fraction	µm	54-105
Temperature	°C	90
V	dm^3	1.5
K_1	1/min	0.001
R^2_1		0.9795
K_2	1/min	0.0003
R^2_2		0.9939

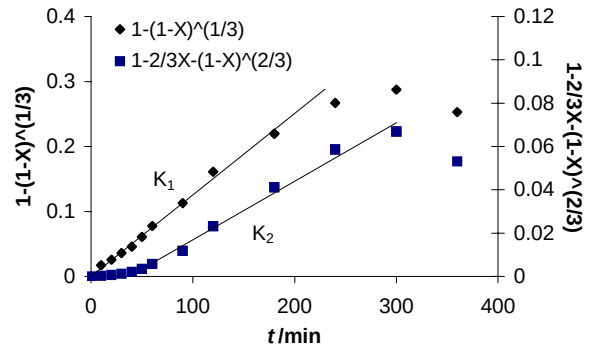

Measurement		M16
Fe (III)	mM	75
Fraction	µm	54-105
Temperature	°C	90
V	dm^3	1.5
K_1	1/min	0.0013
R^2_1		0.9954
K_2	1/min	0.0003
R^2_2		0.986

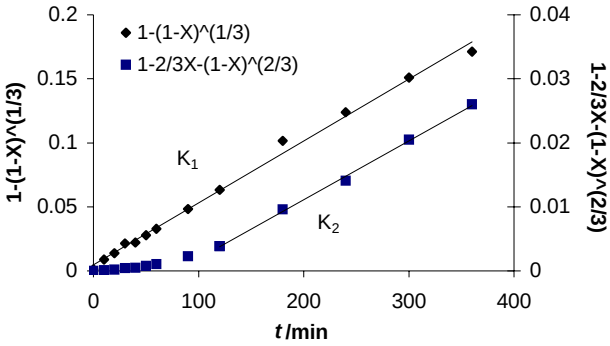

Measurement		M12
Fe (III)	mM	33
Fraction	µm	54-105
Temperature	°C	60
V	dm^3	1.2
K_1	1/min	0.0005
R^2_1		0.9953
K_2	1/min	0.00009
R^2_2		0.9977

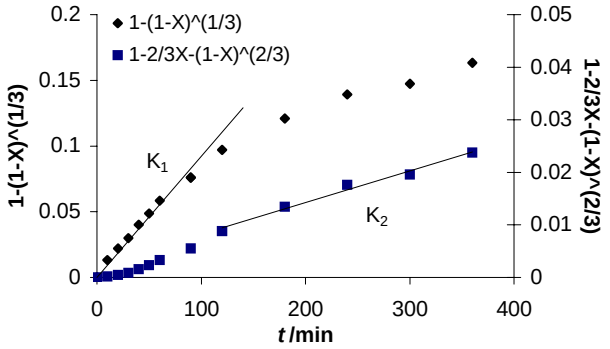

Measurement		M13
Fe (III)	mM	33
Fraction	µm	54-105
Temperature	°C	70
V	dm^3	1.2
K_1	1/min	0.0009
R^2_1		0.9753
K_2	1/min	0.00006
R^2_2		0.9853

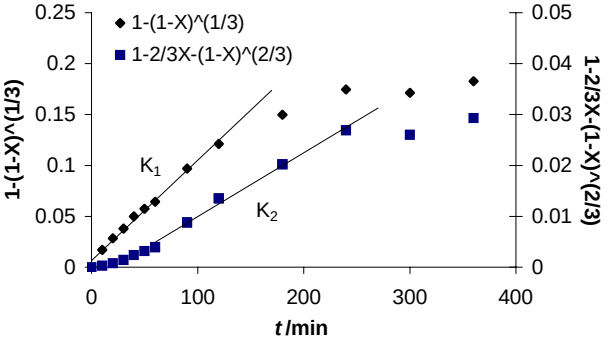

Measurement		M14
Fe (III)	mM	33
Fraction	µm	54-105
Temperature	°C	80
V	dm^3	1.2
K_1	1/min	0.001
R^2_1		0.9926
K_2	1/min	0.0001
R^2_2		0.9928

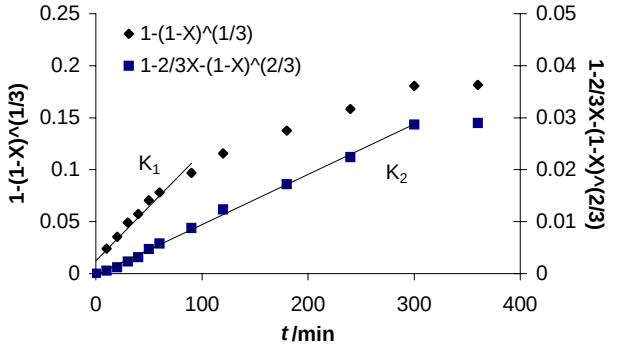

Measurement		M15
Fe (III)	mM	33
Fraction	µm	54-105
Temperature	°C	90
V	dm^3	1.2
K_1	1/min	0.001
R^2_1		0.9516
K_2	1/min	0.0001
R^2_2		0.9978

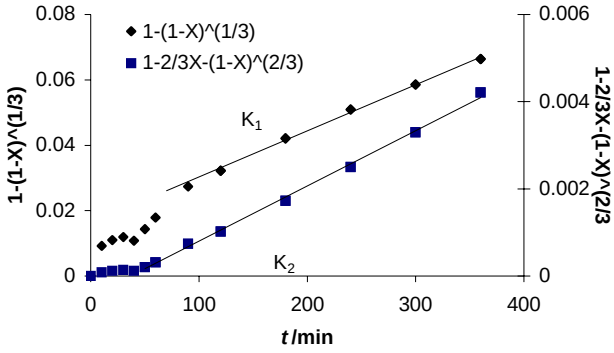

Measurement		M17
Fe (III)	mM	75
Fraction	µm	54-105
Temperature	°C	60
V	dm^3	1.2
K_1	1/min	0.0001
R^2_1		0.997
K_2	1/min	0.00001
R^2_2		0.9977

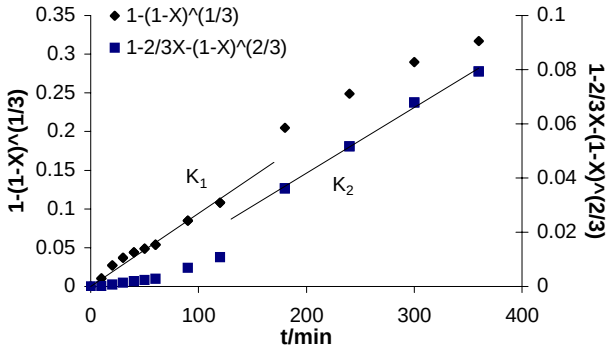

Measurement		M18
Fe (III)	mM	75
Fraction	µm	54-105
Temperature	°C	70
V	dm^3	1.2
K_1	1/min	0.0009
R^2_1		0.9865
K_2	1/min	0.0002
R^2_2		0.9949

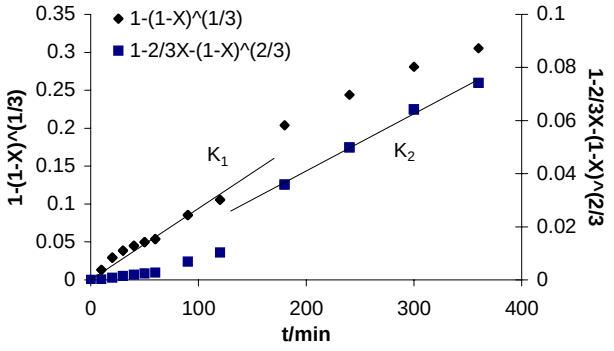

Measurement		M19
Fe (III)	mM	75
Fraction	µm	54-105
Temperature	°C	80
V	dm^3	1.2
K_1	1/min	0.0009
R^2_1		0.9596
K_2	1/min	0.0002
R^2_2		0.9941

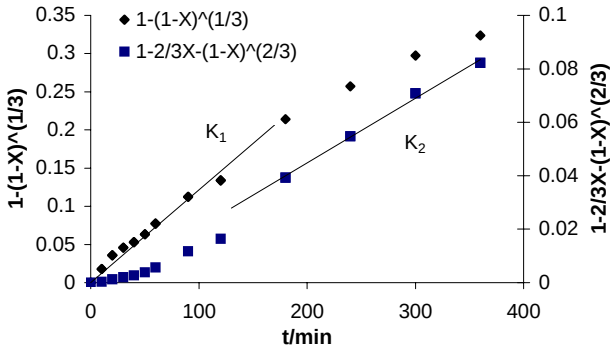

Measurement		M20
Fe (III)	mM	75
Fraction	µm	54-105
Temperature	°C	90
V	dm^3	1.2
K_1	1/min	0.0012
R^2_1		0.9696
K_2	1/min	0.0002
R^2_2		0.9945